UNIVERSITY OF GUANAJUATO

DIVISION OF SCIENCES AND ENGINEERING

CAMPUS LEÓN

BIOPHOTONIC AND MOLECULAR ANALYSIS OF TUBULINOPATHIES

THESIS

TO OBTAIN THE:

MASTER'S DEGREE IN APPLIED SCIENCES

Author:

Carla María Jaramillo Restrepo, Biomed. Eng.

Advisors:

Víctor Hugo Hernández González, M.D., PhD.

Silvia Alejandra López Juárez, PhD.

Index

Abbreviations

H-ABC: Hypomyelination with Atrophy of the Basal Ganglia and Cerebellum.

CNS: Central Nervous System.

OL: Oligodendrocyte.

MTs: Microtubules.

MTAs: Microtubule Targeting Agents.

WT: Wild Type.

PhC: Phase Contrast.

PTX: Paclitaxel.

Epo: Epothilone.

NDZ: Nocodazole.

ROI: Region of interest.

Table of figures

Abstract

In this work, we analyzed the cytoskeleton changes produced by drugs that affect microtubular dynamics on three cultured human cell lines to generate molecular models to explain the pathophysiological processes that give rise to hypo-demyelination and central malformations of the H-ABC tubulinopathy. Tubulinopathies are diseases characterized by mutations in the genes that code for tubulin; specifically, mutations in TUBB4A produce hypomyelination with atrophy of the basal ganglia and cerebellum (H-ABC). Clinically, it is characterized by spasticity, extrapyramidal movements, ataxia, and cognitive and sensory deficits. Morphologically it has been observed that oligodendrocytes (OL) present an abnormal abundance of microtubules (MTs). The molecular mechanisms that trigger these cytoskeletal alterations are unknown, so their study will allow us to understand the pathophysiological processes that give rise to hypo-demyelination and the characteristic central malformations of H-ABC.

We found that paclitaxel and epothilone B (Epo B) induced a higher tubulin density, thus suggesting that treatment with these drugs could generate microtubular behavior, similar to that observed in OL from patients with H-ABC.

These results allowed us to have a better understanding of H-ABC disease, since the changes produced by these drugs in MTs can be used as pharmacological models to study the structural modifications that occur in the cytoskeleton of patients with this disease.

As future work, OLs with and without the mutation will be exposed to different drugs that affect the dynamics of MTs. These experiments will allow mimicking the microtubular defect observed in H-ABC, which will be analyzed later using other microscopy techniques, such as electron microscopy, following the MTs in detail.

Introduction

Tubulinopathies

Tubulinopathies are a group of recently described diseases characterized by mutations in tubulin isotypes (TUBB4A, TUBA1A, TUBB2A, TUBB2B, TUBB3, TUBB, and TUBG1), which in turn, cause neurodevelopmental and neurodegenerative disorders [1], [2].

H-ABC disease

Hypomyelination with atrophy of the basal ganglia and cerebellum is a particular case of tubulinopathy, caused by mutations in TUBB4A which is expressed mainly in OLs. More than 40 mutations have been reported in the *TUBB4A* gene [2]. It is clinically characterized by extrapyramidal movement abnormalities, spasticity, cerebellar ataxia, and sometimes epilepsy [3]. These extrapyramidal movement disturbances are often a remarkable feature of H-ABC because cerebellar ataxia and spasticity are the typical manifestations of hypomyelination. The presumptive diagnosis of H-ABC is made by magnetic resonance imaging [4] which is corroborated by genetic tests.

Our laboratory described the first case of this tubulinopathy in Mexico, and two mutations in TUBB4A were evidenced, one that generates the H-ABC disease in humans (D249N) [5] and the other one in an animal model, the *taiep* rat (A302T). In this rat OLs, there is an abnormal abundance of MTs [6]. They are arranged in linear rows, either alone or aligned around the endoplasmic reticulum and the outer nuclear envelope *(Fig.1)* [7]. This microtubular defect affects the myelinating capacity of the OLs.

The classic H-ABC mutation in humans, c. 745G> A (p.D249N), locates in the T7 loop in the protein, involved in the longitudinal contacts of tubulin. The D249 residue is close to the GTP site and is believed to play an important role in the interaction between the T7 loop and α-tubulin-bound GTP. It has also been reported that other mutations close to GTP, such as p.A352T, p.C354Y, and p.M323R, cause the typical phenotypes of H-ABC [8].

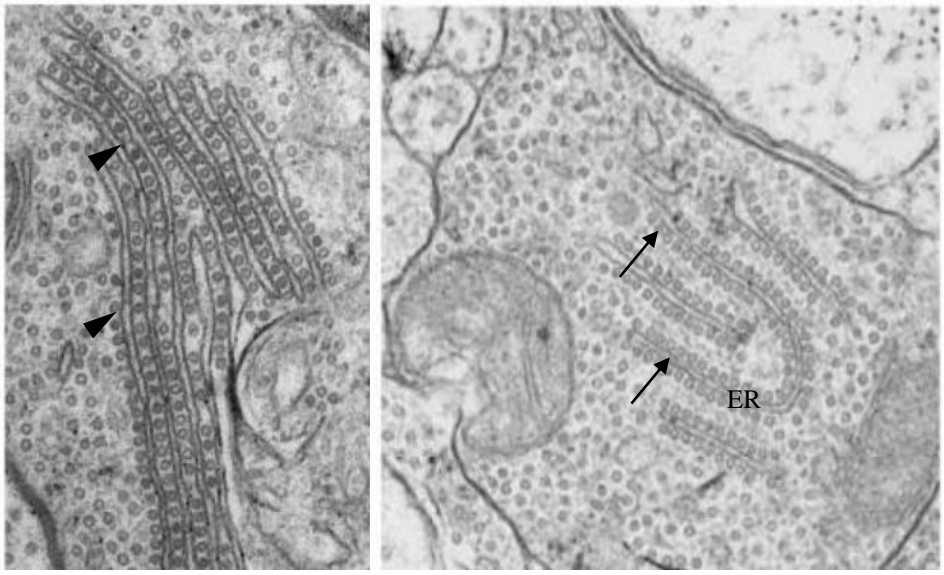

Figure 1. Transmission electron micrographs of OLs in the taiep rat. *right OLs contain packed microtubules linking adjacent (arrowheads) or aligned with endoplasmic reticulum (ER) (arrows)* [7].

MTs are part of the cell cytoskeleton, and therefore they are involved in essential processes for the maintenance of the cell, for example, a) proliferation, since they participate in mitosis, allowing the correct separation of chromosomes; b) cellular functionality depends on the cytoskeleton for the intracellular transport of proteins, organelles, and vesicles; and c) cell fate, the migratory capacity of a cell depends on the proper functioning of the MTs [9]. MTs are characterized by their dynamic, which varies between growth (polymerization) and shortening (depolymerization) processes. A disruption in these mechanics generates major failures in the maintenance of the cytoskeleton and microtubule-dependent transport.

Structure and formation of MTs

The structural and functional subunit of the MTs is a heterodimer of two highly conserved globular proteins, namely α- and β-tubulin. The α- and β-tubulin dimers polymerize to form 13 laterally associated protofilaments constituting a polar hollow cylinder [10] composed of two ends, a plus-end (increasing) and a minus end (depolymerizing). The structures of α- and β-tubulin are highly conserved throughout eukaryotes, and therefore the structural conformation of longitudinal protofilaments is tightly regulated [11].

The lateral contacts are homotypic (α-α and β-β), except in a single site or "seam" (α-β and β-α) *(Fig.2),* and their functional relevance is not yet understood, although it seems to be linked to the ring structure of γ-TURC explained later [10]. Polarity will determine the direction of the molecular motors along the MTs, and an alteration in this property will have significant consequences in their conformation.

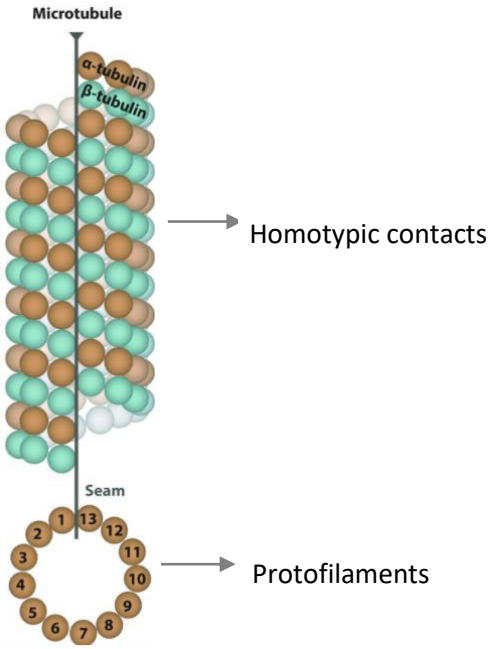

Figure 2. Schematic of a microtubule, showing the seam [72].

MTs undergo rapid assembly and disassembly cycles through polymerization and depolymerization of tubulin dimers. Each tubulin monomer binds to a guanosine 5'-triphosphate (GTP) molecule, not exchangeable in α-tubulin (N-site) and interchangeable in β-tubulin (E-site). GTP bound to β-tubulin hydrolyzes to GDP immediately after polymerization, thus weakening the binding affinity between tubulin dimers and causing depolymerization, that is, a rapid loss of GDP-bound tubulin molecules at the plus end.

The correct intracellular organization of the MTs involves the participation of the central organizing center of the MTs or centrosome, where the minus ends join. From there, they start their growth towards the cell periphery. It is the initiation of MTs growth in the centrosome that establishes their polarity in the cell. The main component of the centrosome is another tubulin, γ-tubulin, associated with other proteins to compose a ring-shaped structure known as the γ-tubulin ring complex (γ -TURC) [11] *(Fig 3).*

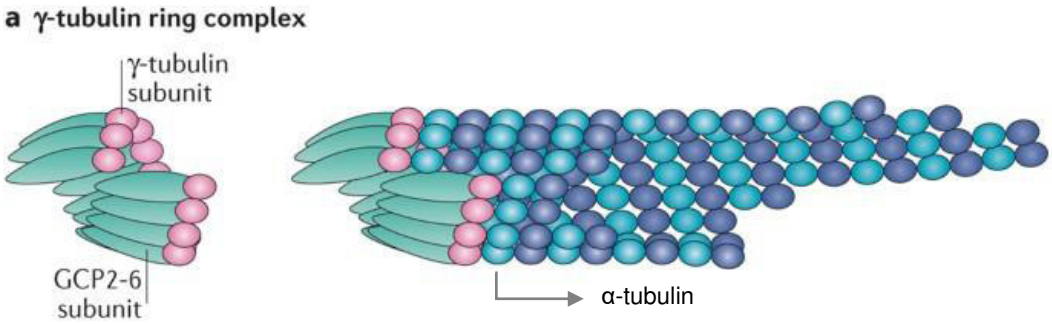

Figure 3. Microtubule nucleation scheme from the γ-tubulin ring complex. *The γ-tubulin subunits (pink) are arranged into a pseudo-helical conical structure that caps the microtubule minus ends and interacts with the alpha tubulin (blue). Modified from* [17].

In the cell, the minus end of the MTs is composed of α monomers, anchored to the γ-TURC. In the plus end, β-tubulin monomers are the most dynamic [12] *(Fig. 4A)*. GTP must be present at the E-site for tubulin to polymerize, but if it is hydrolyzed to GDP, the MTs are in a metastable structure *(Fig. 4B)*. It is the accelerated hydrolysis of GTP at the end plus that results in rapid depolymerization. Therefore, the stability of the MTs is determined by the presence or absence of tubulin-GTP at the + end (GTP-CAP). The existence of this cap will determine whether the MTs will grow or depolymerize, and this characteristic gives rise to the process known as "dynamic instability," an essential property of MTs [13], [14] *(Fig. 4C)*.

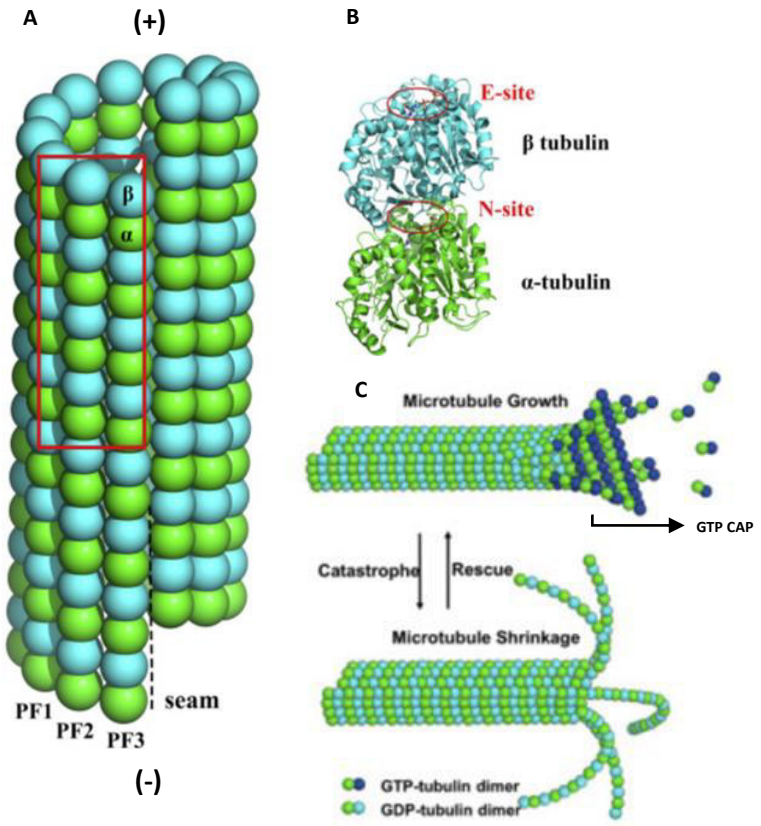

Figure 4. Instability dynamic of MTs ***(A)*** *Schematic view of the MTs structure.* ***(B)*** *Shown is a cartoon representation of the α-β tubulin heterodimer, which serves as the basic building block of the MT. The nonexchangeable nucleotide binding site (N-site), located at the intradimer interface, can only bind GTP molecules. In contrast, the E-site, exposed at the top of β tubulin domains, can bind either GTP or GDP molecules.* ***(c)*** *Illustration of MTs dynamic instability. MTs can switch between the growth state and shrinkage state, depending on the presence of the GTP cap* [73].

MTs growth continues as long as there is a high concentration of GTP-bound tubulin. In this case, the GTP-bound tubulin molecules are added faster than the GTP is hydrolyzed, thus maintaining a GTP cap at the growing end (+). On the other hand, if the GTP is hydrolyzed faster than the new subunits are added, the presence of tubulin bound to GDP leads to disassembly and shortening [11]. Both *in vivo* and *in vitro*, the plus end of MTs undergoes such commutations between growth and depolymerization phases. This characteristic behavior is a vital property for cell function, especially during mitosis, as highlighted, for example, agents against cancer such as paclitaxel (PTX) inhibit cell division by stabilizing MTs and suppressing their particular "dynamic instability" [10].

Microtubule-associated proteins (MAPs) regulate the dynamic behavior of MTs. Based on their mode of action, MAPs can be classified into (a) motile MAPs, motor proteins that generate forces and movement [15], (b) enzymes that break or depolymerize MTs [16], (c) microtubule nucleators, and [17] (d) end-binding proteins that specifically associate with

plus- or minus-ends of MTs [18]. In turn, the growth or shortening of the end plus is regulated by MAPs that promote the polymerization or depolymerization of tubulin dimers. The polymerases bind to the end plus and multiply their growth rate by increasing the incorporation of tubulin-GTP. The depolymerases stimulate its shortening by accelerating the dissociation of tubulin-GDP. In turn, another class of MAPs called CLASP (CLIP-associating proteins) suppress the catastrophe and promotes the rescue of MTs by stopping their disassembly and restarting their growth [11].

To incorporate subunits of alpha and beta-tubulin into the MTs, the transformation of GDP to GTP in β-tubulin is required. These heterodimers then assemble head-to-tail to compose an initially open sheet of polar longitudinal protofilaments. The lateral interactions between the filaments cause the passage of an open sheet to form a hollow tube. MAPs interact with the outer surface of MTs to regulate their dynamic property and stability, as well as motor proteins (dynein and kinesin) that also bind in these regions.

Due to the large number of functions in which MAPs are involved, it is not surprising that they are also involved in various pathological conditions [19]. It has been reported that transgenic mice for mutant/missing MAPs are models supporting MAPs structure maintenance and functions of the mammalian brain relevance [20]. In this regard, it is known that mutations located in the outer helices of tubulins will affect the correct interaction with these proteins *(Fig. 5).*

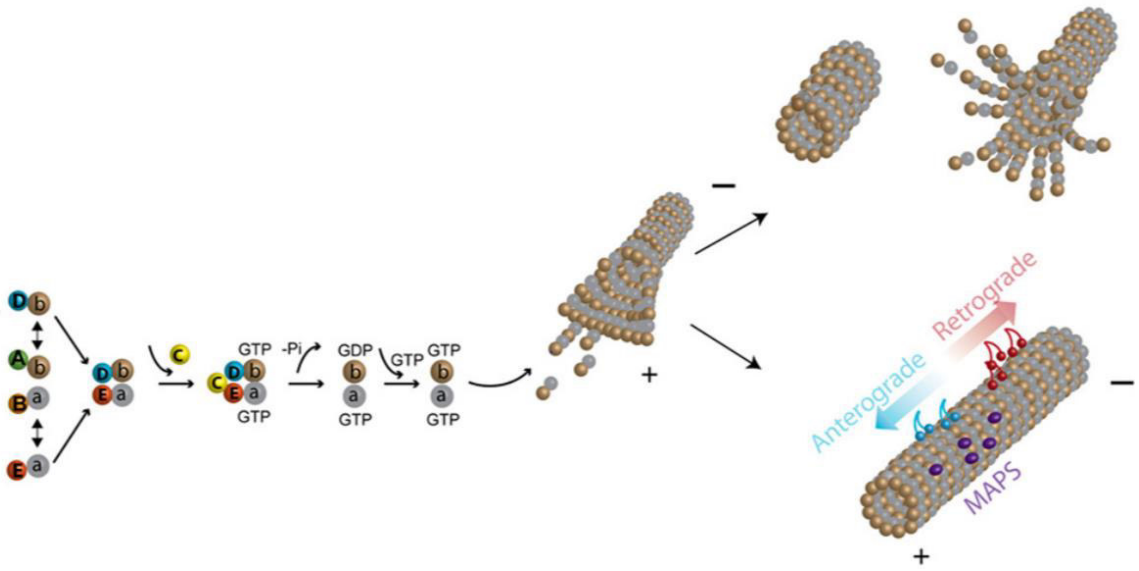

Figure 5. Folding of tubulin heterodimers and interactions with MAPs and motor proteins. *The brown spheres represent the β-tubulin monomers, the gray spheres represent the α-tubulin monomers. The rest of the spheres symbolize the chaperones that collaborate in the stability and formation of the heterodimer* [24].

Structural domains in tubulins

The α- and β-tubulin monomers are very similar in their compact structure. The secondary and tertiary structures of the monomers are essentially identical. There is 40% of identity in their sequence of approximately 450 amino acids [21]. Each monomer comprises three sequential and functionally distinctive domains: N-terminal, intermediate, and C-terminal domains *(Fig.6).* Each of them is composed of both α-helix structure and β-chains, and they develop at least six different functions participating in the stability of the heterodimer, longitudinal and lateral interactions of the protofilament, nucleotide exchange and hydrolysis, and the protein-microtubule interactions.

The N-terminal region is formed by six parallel β chains (S1 – S6) that alternate with helices (H1 – H6). In this way, each loop (T1-T6) is composed by the end of a strand joined at the beginning of the subsequent helix, directly involved in interactions with the nucleotide. The GTP-binding pocket is a vital structure for the folding, the design and the stability of tubulin heterodimers, as well as for the assembly of protofilaments and their necessary lateral interactions for the final structure of the MTs [21], [22].

In the intermediate domain, the loops H6–H7, T7, and the helix H8 fall in the longitudinal intra- and inter-dimer interfaces during MTs assembly. The loop T7 interacts with the nucleotide of the next subunit along the protofilament [2].

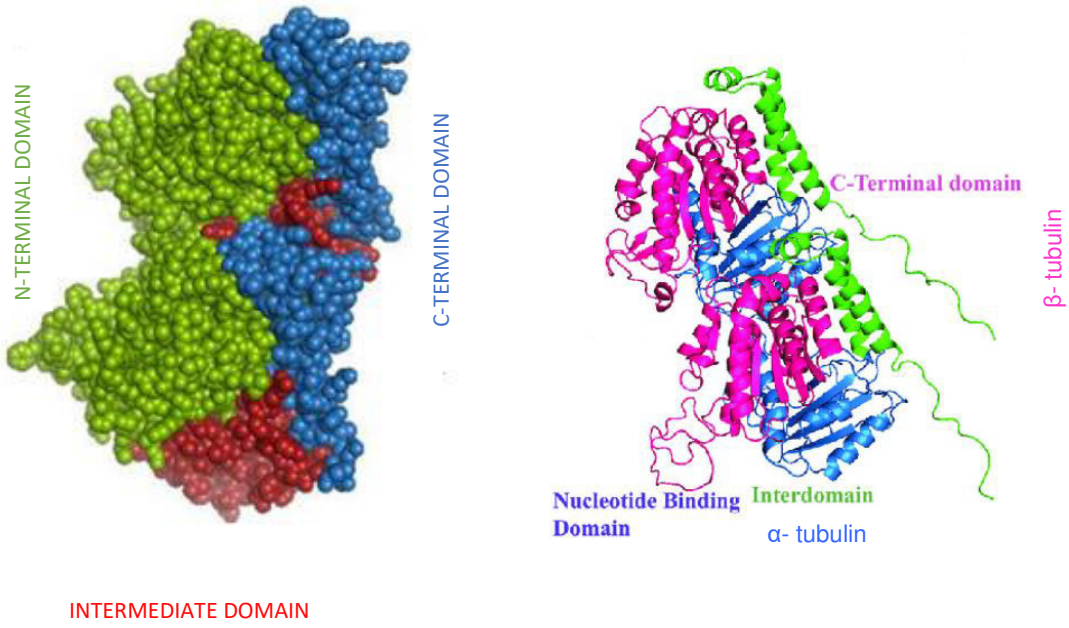

Figure 6. functional domains and 3D structure of the tubulin heterodimer*. Left shows the three structural domains of tubulin heterodimer. The N-terminal domain includes the first 205 residues. The intermediate domain comprises residues 206-381 and the C-terminal domain is made up of two structures, which overlap on the N-terminal and intermediate domains. This domain appears to be involved in the binding of MAPs and motor proteins. Right* **corresponds to the three-dimensional structure of tubulin heterodimer:** α- tubulin (blue) and β- tubulin (pink) *[23], [71].*

The N site is formed principally by α-tubulin residues; there, GTP is buried in the intra-heterodimeric interface between the two monomers, which prevents it from been hydrolyzed to GDP. On the other hand, the E-site is composed of residues located at the plus end of β-tubulin; therefore, it is partially exposed on the surface of the dimer. Thus, GTP from β-tubulin may eventually hydrolyze when heterodimers are incorporated into the MTs (*Fig.7)* [24].

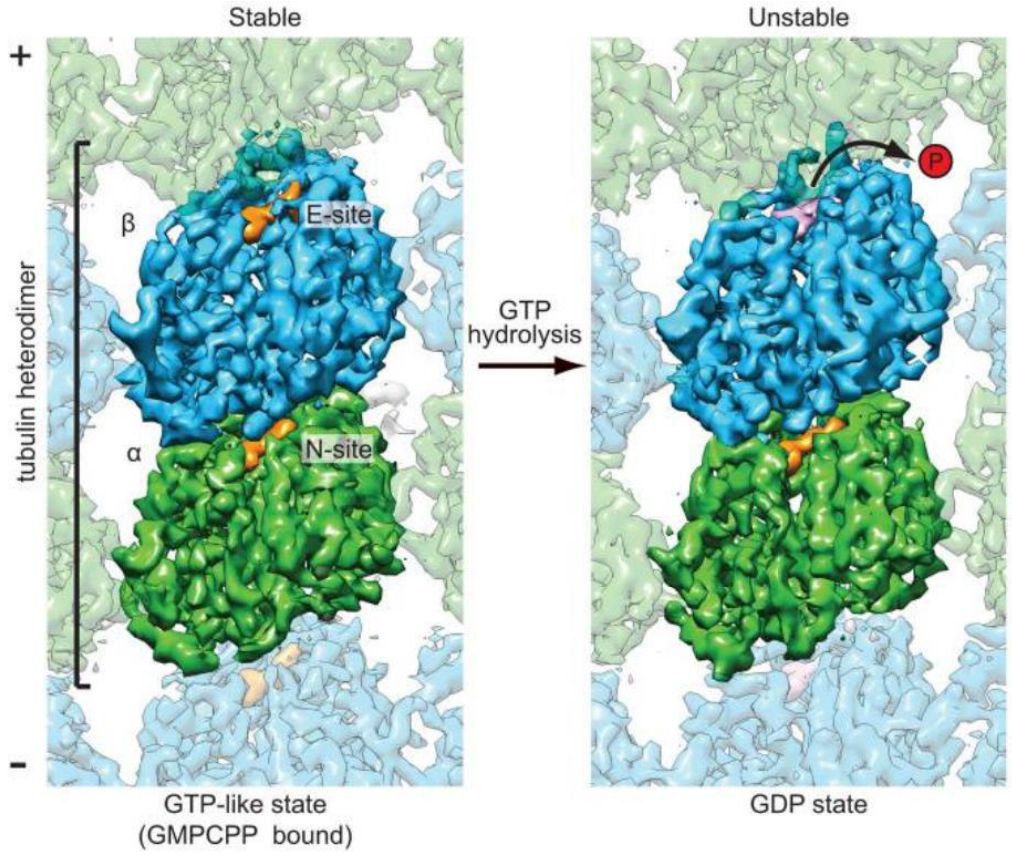

Figure 7. Representation of the tubulin heterodimer. *The GTP of α-tubulin (N-site) and the GDP of β-tubulin (E-site). It can be seen how the GTP of α-tubulin is buried in the intradimeric face, while the GDP of β-tubulin is exposed on the surface of the dimer* [75].

The C-terminal domain is formed mainly by two antiparallel helices (H11-H12) that cross the other domains [12]. The α helices contain residues that are important for the stability of the protofilaments. Motor proteins bind directly to the helices exposed in the outer surface, allowing correct intracellular transport and, in turn, other MAPs extrinsically control microtubular dynamics [25], [26].

Intermediate domains allow the interactions necessary for stability between the monomers within the heterodimer and the MT. Other residues of the intermediate domain interact with adjacent N-terminal domains to participate in structural rearrangements of GTP hydrolysis products within β-tubulin. When this hydrolysis occurs, the heterodimer turns from its initial straight structure to an open curve that favors depolymerization [22], [27].

Longitudinal interactions are mediated by highly conserved residues located in the inter and intra-heterodimeric regions. Their primary function is to preserve the dimer's stability and the protofilament's assembly. Lateral interactions between the protofilaments are made by residues located on the lateral and internal faces of the heterodimer. They are essential to

compress the protofilament sheet into a definitive hollow cylindrical structure and regulate the MT's dynamics [24].

Microtubule Targeting Agents (MTAs).

Besides the importance of the dynamic properties of MTs for several cellular functions, e.g., the transport of intracellular organelles and the development and maintenance of cell shape, they are also essential for the mitotic spindle formation during mitosis [28].

The MTs of the mitotic spindle are between ten and one hundred times more dynamic than during the interphase [29]. This is essential for the correct anchorage of the chromosomes to the spindle after the rupture of the nuclear membrane during prometaphase [30] and for the complex movements that align them in the metaphase plate. In addition, the MTs of the mitotic spindle are also necessary for their synchronized separation during anaphase and telophase after the metaphase-anaphase checkpoint has been completed [31]. Thus, an alteration in the dynamics of the MTs affects all these functions. Consequently, the normal progression of the cycle is blocked, leading the cell to apoptosis [32] *(Fig 8).*

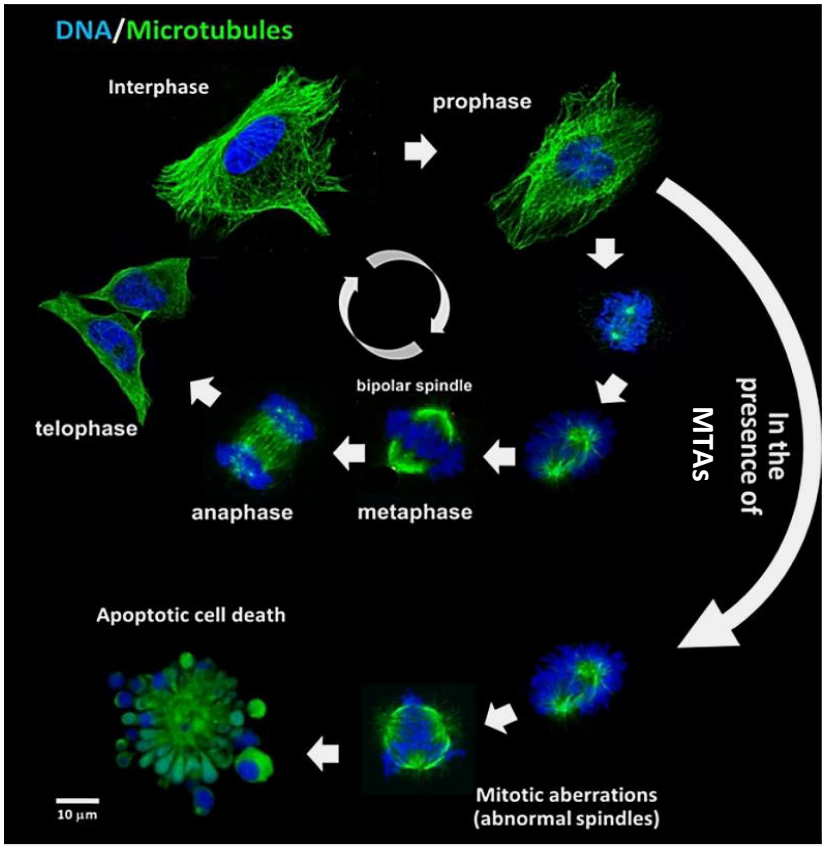

Figure 8. Microtubule changes during the cell cycle and mitotic aberrations. *The behavior of the MTs (shown in green), changes throughout the cell cycle, being very dynamic during mitosis and with a slower dynamic at interphase. MTAs cause a mitotic arrest at metaphase, inducing apoptosis upon exit from the cell cycle. Adapted from* [76].

MTs are targets for treatment of cancer, because an alteration in their dynamics can activate the spindle checkpoint, stopping the progression of the cell cycle in mitosis and eventually lead to apoptotic cell death [33].

The discovery of microtubule-binding drugs date back some 50 years [34], when vinca alkaloids were isolated from the leaves of Madagascar flower (*Catharanthus roseus*) and used like agents against cancer. Conventionally, antimitotic compounds directed against MTs are classified into two groups: stabilizers and destabilizers [35]. It has been reported that high concentrations of stabilizing agents induce MTs polymerization [36], while destabilizers inhibit its polymerization, favoring depolymerization.

The specific effects of each of these compounds on MTs mass, stability, and dynamics are quite complex and vary from one to another. Therefore, they have been classified based on their binding sites *(Fig. 9),* in addition to their effect on MTs. Most MTAs bind one of four main sites/domains within MTs impacting tubulin stability:

Binding sites of MTAs				
Effect on microtubule	laulamide	Taxane/epothilone	colchicine	vinca
		stabilizing		destabilizing

Table 1. Binding sites of MTAs to tubulin and their effect on MTs [77]

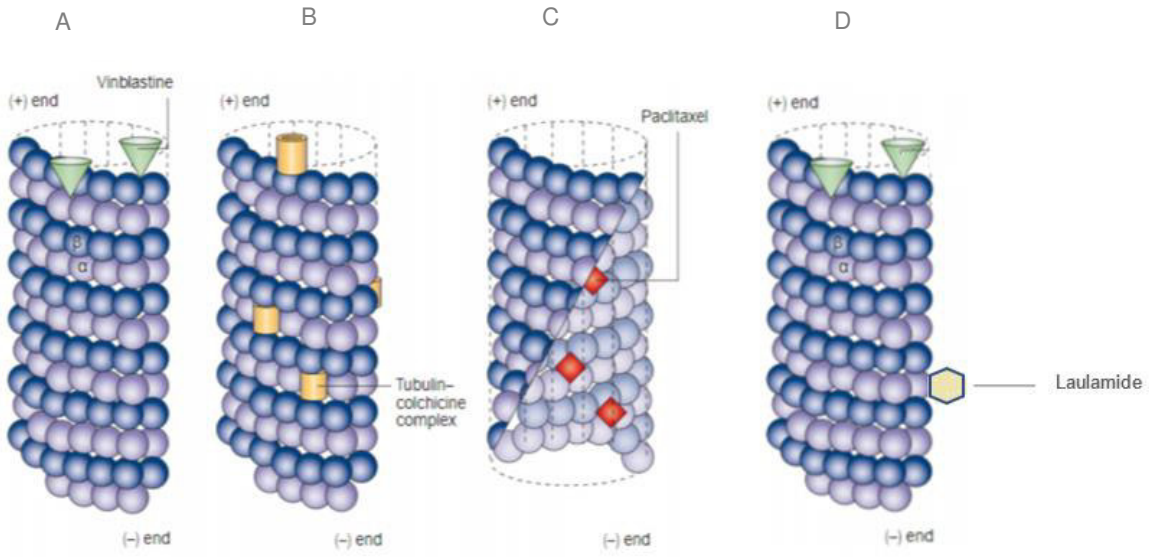

Figure 9. Tubulin binding sites of microtubule targeting agents. A *Molecules of vinblastine bound to high affinity sites at the positive ends of the MTs.* ***B*** *Colchicine complexes with tubulin dimers and copolymerizes in the network of MTs.* ***C*** *a cut microtubule is shown to view the inner surface and show PTX binding sites.* ***D*** *laulimalide site is shown in alpha tubulin (yellow). Adapted from* [31].

The site of paclitaxel

Paclitaxel (PTX), isolated from the bark of the Pacific yew tree *Taxus brevifolia* was the first microtubule-stabilizing agent described [37]. This MTA has its binding site in the lumen of the MT, near to the lateral interface between protofilaments *(Fig. 9C).* It is believed to have access by diffusing through small openings or fluctuations in the protofilament network that make its passage possible. It binds to GDP-bound β-tubulin and induces a change in its conformation to GTP-bound β-tubulin, which is more stable than the former. In this way, PTX stabilize the MT, thus favoring its polymerization [38].

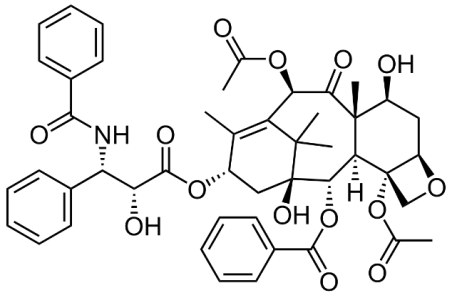

Figure 10. Structure of PTX.

Recently, several high-resolution cryo-electron microscopy studies comparing MTs in different nucleotide states have reported that GTP hydrolysis generates compaction at the longitudinal interdimeric interface, contiguous to the nucleotide in β-tubulin [39]. PTX appears to reverse, at least partially, the effect of GTP hydrolysis, leading to a more expanded network after GTP hydrolysis. However, its mechanism of action at the longitudinal interface has not been detailed [40].

At the amino acid level, the binding site for PTX resides in a deep hydrophobic cleft near the surface of the β (where the A302T mutation of the *taiep* rat localizes), where it interacts with the protein through three hydrogen bonds. Helix segments H1, H6, H7, and the loop between H6 and H7 interact with 3'-benzamido phenyl, 3'-phenyl, and 2-benzoyl phenyl of PTX. In addition, 3'-phenyl has close contact with the β-sheet strands B8 and B10. Therefore, it interacts with the following tubulin amino acids: [Leu-230, Ala-233 (H7); Phe 272, Pro-274, Thr-276, Leu-286, Leu-291 (M loop); Pro-360, Leu-371 (loop B9-B10); and Ser-374 (B10)] *(Fig 11)* [41].

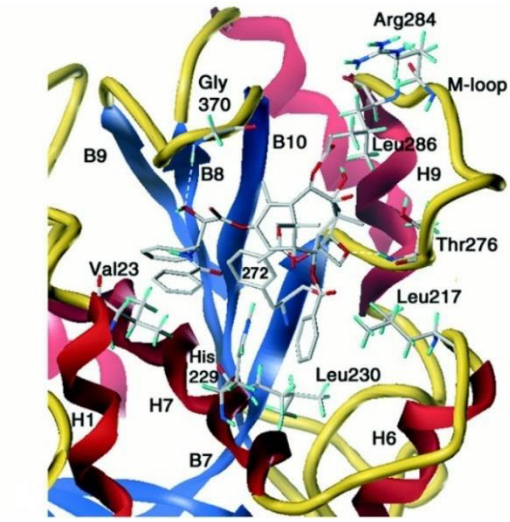

Figure 11. Binding interactions between PTX and B-Tubulin [41].

New antimitotic agents that bind to the PTX site

Epothilones

Epothilones are macrolactones, originally isolated from the myxobacterium *Sorangium cellulosum*. These agents induce mitotic arrest by suppressing MTs dynamics, and the comparison of the effects of Epothilone (Epo) B on MTs dynamics with those of PTX indicated that both drugs alter the same MTs dynamic parameters to a similar extent [42]. Epothilones favor the polymerization and subsequent stabilization of MTs.

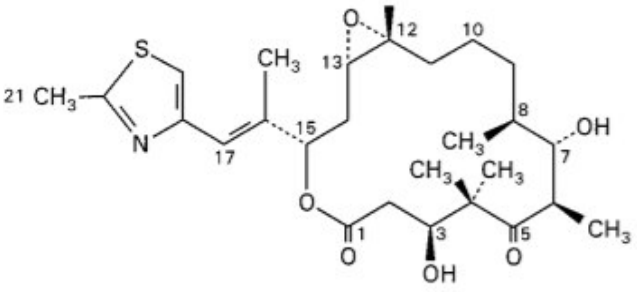

Figure 12. Structure of Epothilone B.

Epothilones are more soluble in water than PTX, eliminating the need for a vehicle, as in PTX treatment. Therefore, they are more effective against PTX-resistant cells that overexpress P-glycoprotein, a membrane efflux pump that significantly decreases intracellular PTX concentrations [43]. On the other hand, Epo B has the same effects as PTX on *in vitro* purified MTs and on mitotic spindle structure and function in cell culture. Both drugs alter the same MTs dynamic parameters and to a similar degree, causing mitotic arrest during metaphase [44].

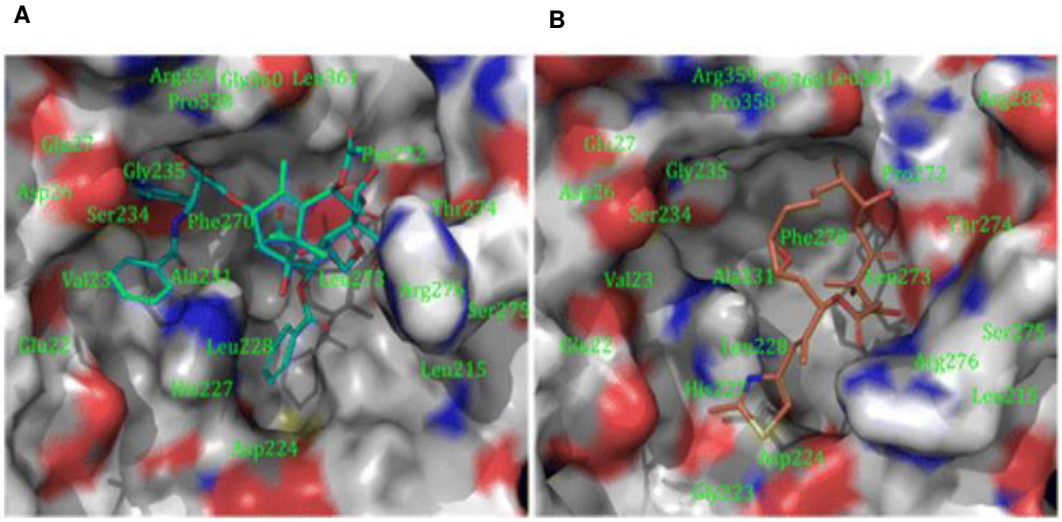

Figure 13. Electron-crystallography-derived 3D models of (A) *PTX (cyan carbon) and* ***(B)*** *Epo B (brown carbon) bound to zinc-stabilized α, β-tubulin sheets. Colors represent elements: gray = C and H, blue = N, red = O, and yellow = S* [47].

Epo B shares the same binding site as PTX to B-tubulin *(Fig 13 A),* except for some amino acids [45]. Recently, a model of the conformation and binding mode of Epo B was reported, based on electron crystallography of Zn^{2+} induced tubulin sheets [46]. *Fig 13* B shows the interaction of Epo B with tubulin, which forms hydrogen bonds with Arg282, Thr274 and Arg276, and thiazole nitrogen with His227 on the H7 helix.

Both PTX and Epothilones cause stiffness and alignment of the M loop and H7 helix leading to a conformational change in the α, β-tubulin dimer. This mechanism explains its stabilizing effect on MTs after GTP hydrolysis [47].

The site of Colchicine

Colchicine

Colchicine was extracted from the poisonous meadow saffron *Colchicum autumnale.* Colchicine binds with high affinity to tubulin, which can copolymerize into MTs. The binding of colchicine to β-tubulin results in a curved tubulin dimer and prevents it from adopting a linear structure due to steric shock between colchicine and α-tubulin, which inhibits MTs assembly [48].

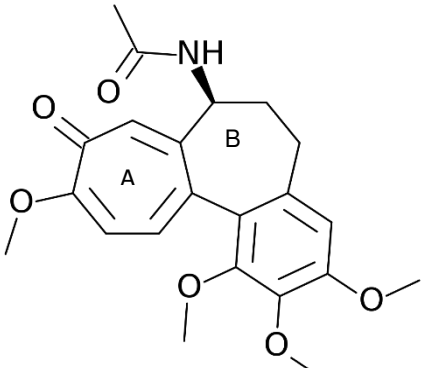

Figure 14. Structure of colchicine.

Colchicine binds with high affinity to the β subunit, interacting mainly with H7. Cys-241 forms hydrogen bonds with the trimethoxy phenyl ring of colchicine (ring A, *Fig 15*), while Thr-179 and Val-181 within α-tubulin form hydrogen bonds with the tropolone ring (ring B) (*Fig 15)* [49].

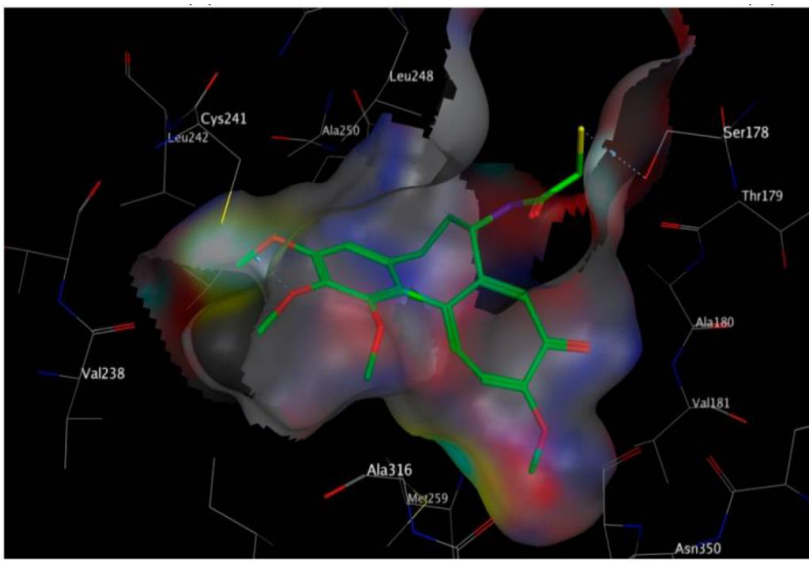

Figure 15. Binding site of colchicine and tubulin [49].

Nocodazole (NDZ)

NDZ is an antimitotic drug discovered as part of an effort to find effective agents against the helminth parasite *Ascaris lumbricoides*. NDZ belongs to a group of competitive inhibitors of colchicine binding to tubulin [48]. This drug has been reported to bind with high affinity to tubulin and inhibit MTs assembly [50].

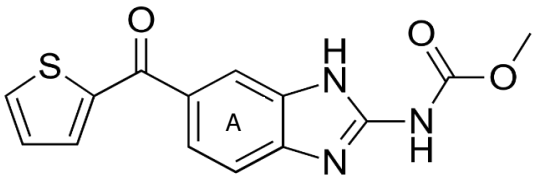

Figure 16. Structure of NDZ.

Although the binding site of NDZ overlaps with that of colchicine, the two drugs are structurally quite different [51]. NDZ, for example, does not have a trimethoxy phenyl ring, typical of many colchicine-site binders. It is thought that the phenyl *(Fig 16A)* group may act in the same role and bind to the same site as the trimethoxy phenyl ring of colchicine [52].

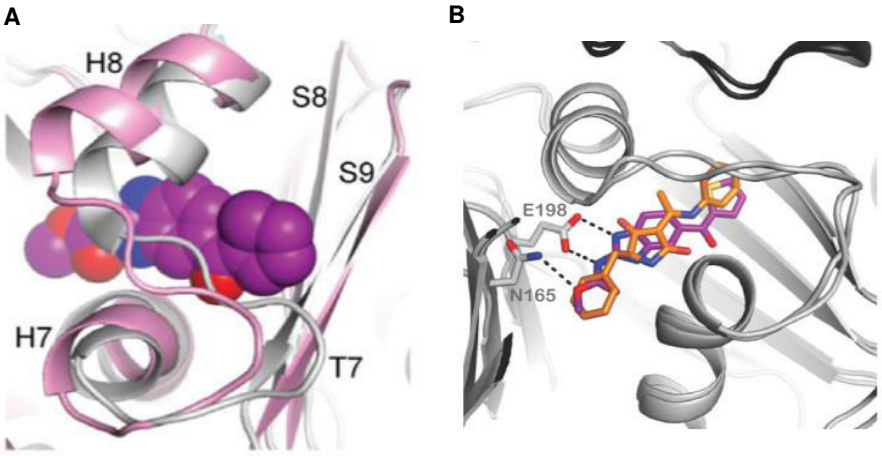

Figure 17. Interaction between NDZ and tubulin. *A superimposition of the drug and tubulin as found in straight protofilaments. B interaction with amino acids of tubulin* [54].

Recently, a coupling model based on drug resistance-associated mutations has placed NDZ in a deeper pocket of β- tubulin [53]. It interacts via hydrogen bonding with N165 in S5 and E198 in S6 *(Fig 17B). Fig. 17A* shows the superposition of the NDZ molecule (sphere representation) and tubulin as found in straight protofilaments. The drug's interaction with S8, S9, H7, T7, and H8 is evidenced [54], indicating its proximity to the classic H-ABC (D249N) mutation site in T7 [2].

Even though all these drugs affect MTs dynamics differently, they attach tubulin close to the sites of the most frequent mutation of H-ABC (D249N) and the mutation in the *taiep* rat

(A302T), which makes them attractive to study the effects of tubulin mutations on the development of tubulinopathies.

At the cellular level, mutations in the TUBB4A gene exhibits an accumulation of MTs in the oligodendrocytes; however, the molecular mechanisms responsible for this microtubular defect have not been described. In this work we focus on providing a pharmacological model that will allow us to understand the pathophysiological processes that give rise to hypo-demyelination and central malformations characteristic of H-ABC.

General Objective

To develop an *in vitro* pharmacological model that allows understanding the molecular processes in MTs due to mutations in TUBB4A.

Specific objectives

a) To characterize the concentration of each drug by means of a cell survival test and an analysis of the morphological changes observed by phase contrast microscopy (PhC).

b) To identify changes in the cytoskeleton induced by pharmacological treatment with the proposed drugs through fluorescent tubulin labeling.

c) To determine which drugs, induce a similar phenotype to that occurring in oligodendrocytes carrying the mutations to understand the structural changes present in these conditions.

Materials & methods

Drugs preparation

For cell treatments, we used the following drugs: PTX (Sigma Aldrich, T7402), NDZ (Sigma Aldrich, M1404), colchicine (Sigma Aldrich, C3915) and Epo B (Sigma Aldrich, E2656). Stock solutions were prepared in dimethylsulfoxide (DMSO) to obtain a concentration of 10 mM, 16.66 mM, 125 mM, and 5 mM, respectively. Subsequently, they were diluted in culture medium to obtain final concentrations for cell culture treatments, as indicated in table 2.

	Drugs			
	paclitaxel	epothilone B	nocodazole	colchicine
Concentrations in cell culture	1.25, 2.5 and 5 nM	0.3, 3 and 30 nM	0.1,1 and 10 µM	0.25,2.5 and 25 µM
Incubation time (hr)	12,24,36	15,20,25	6,12,18	4,8,12

Table 2. Concentrations of each drug in cells cultures.

Cell culture

All cell lines we used in these experiments were of human origin¿ SHSY5Y neuroblastoma cells, which express TUBB4A, further differentiate into neurons (a cell type affected by H-ABC) and HEK 293 embryonic kidney cells, which are widely used in biological research as they are easy to grow and have an exponential growth rate. The base medium for HEK 293 cells is Dulbecco's modified Eagle medium (DMEM), and for SH-SY5Y cells DMEM- F12. The complete growth medium contains fetal bovine serum to a final concentration of 10% and 100 µg / ml of penicillin and 100 µg / ml of streptomycin.

The procedure for cell maintenance and passage is detailed in the annexes *(annex 8 page 53).*

Treatment with Drugs

After 48 hours of growth, different concentrations of each drug were added to Petri dishes of 35 mm diameter containing coverslips with adherent cells attached to them as showed in *table 2*. at different times. Subsequently, cells were washed with PBS and trypsinized.

PhC images

Phase-contrast images were taken using the ZEISS microscope, model Axio observer A1, with a 10x or 40x dry objective.

Survival Assay

For cell viability, 600 µl of trypan blue were added to 600 µl of cells resuspended in 1 ml, 15 µl were placed in the Neubauer chamber, and the viable cells were counted.

Details of the survival assay in annexes.

Preparation of cells and immunofluorescence

1ml of PBS at 37°C and 1ml formaldehyde 8% were added to the dish containing the same volume of growth medium (2ml) so the final concentration was 4% formaldehyde and were incubated for 15 minutes. The solution was aspirated, and the coverslips were set in agitation with PBS 3 times for 5 minutes. After that, PBS was removed and 0.1 % triton X-100 in PBS was added for 10 minutes. PBS Triton and a blocking buffer, composed of 10 % Bovine Serum, 0.04% Triton X-100 in PBS, were added for 30 minutes. The staining process was done in a humidified chamber: in a close recipient, a wet paper was placed at the bottom, with parafilm above it. Coverslips were moved to this humidified chamber and placed upside down over 40 µl of medium containing the blocking buffer and antibodies. Every coverslip was incubated upside down over a 40 µl, 1:500 dilution of primary antibody Anti- Tubulin sheep polyclonal (Cytoskeleton, ATN02) in blocking buffer, overnight at 4°C. Then, the coverslips were washed three times with PBS at room temperature for 5 minutes. For two hours, every coverslip was incubated upside down with a 40 µl dilution of 0.2 µl Alexa fluor 488 (Thermo Fisher A-11015), 0.17 µl of DAPI (Thermo Fisher 62247), and 0.8 Alexa fluor phalloidin 647 at room temperature in the dark. Then, the coverslips were set in agitation with PBS for 10 minutes. The minimal volume of fluorescence mounting medium (Prolong Diamond, P36961) was added to the glass slide. The coverslips containing the sample were removed from PBS and dried by tilting the glass on an adsorbent paper. Finally,

the coverslips were placed down onto the mounting medium, avoiding bubbles. The coverslip was sealed with transparent nail polish.

Statistical analysis

A minimum of three repetitions were done for each of the four conditions, i.e., control and three different concentrations of each drug. Two-way ANOVA was applied to determine the concentration or time as significant ($p < 0.05$). Subsequently, a one-way ANOVA was applied (to the variable resulting from the previous test) and, finally, the Tukey test to analyze simple main effects. A bidirectional ANOVA test was used, assuming equal variances. For all experiments, statistical significance was determined by a value of $p < 0.05$.

Based on statistical significance and morphological changes observed by PhC microscopy, the optimal concentration for each drug was selected. After treatment with them, cells were immunostained.

Image acquisition

For fluorescence microscopy, HEK 293 and SHSY5Y slides images were obtained with a LSM 710 Zeiss confocal microscope, using LCI Plan-Neofluar 25x/0.08 Imm Korr DIC M27 and alpha Plan- Apochromat 63X/1.46 Oil Korr M27 immersion objectives. It used FIJI™ to process the images.

Imaging Analysis

Fluorescence density was used as a metric for the analysis of fluorescence in the images obtained. Which corresponds to the fluorescence intensity/number of pixels of each ROI (Region Of Interest). Python was used for the analysis.

Details of procedure in the annexes (annex 9 *page 53*).

Determination of dose and exposure time for each drug

For the characterization of each drug, two parameters were considered: a) morphological changes observed by PhC microscopy and b) the effects on cell survival. The range of pharmacological dose/time to induce the effect of drug in each cellular type was obtained from the literature. The cell cultures were treated with three different concentrations at different incubation times. The survival data were analyzed to determinate the better conditions (concentration and time) for each cellular type. Then, the effect on MTs were analyzed by IHF.

1. Stabilization of microtubules induced by PTX reduced the number of cytoplasmic processes in embryonic and neuroblastoma cells at 5nM concentration for 24 hr.

To select the ideal concentration and time for PTX treatment, first the effects of microtubule stabilization on cell proliferation were evaluated. Three different doses of PTX were tested (1.25, 2.5, 5.0 nM) at three time points (12, 24, 36 hr). The cellular survival was evaluated by a cell survival assay. The number of surviving cells at each concentration and time point was plotted in a linear graph for HEK 293 *(Fig. 17A)* and for SHSY5Y *(Fig. 18A).* No significant differences in the number of surviving cells were observed at 12 hr between any tested dose compared to the control.

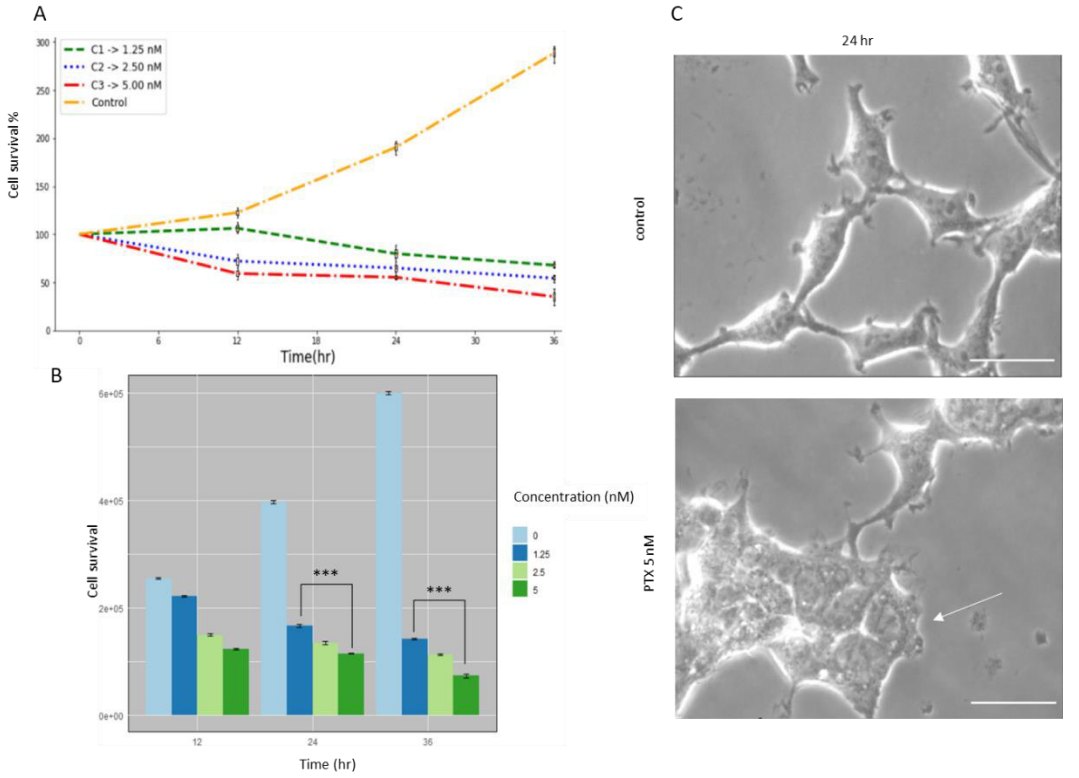

Figure 18. Ideal conditions for treatment with PTX in HEK 293 cells. A *The curves represent the changes in the percentage of cell survival after treatment with different concentrations of PTX at different times.* ***B*** *Bar graphs, showing a significant decrease (*** *P <0.05) in cell survival for PTX 1.25, 2.5 and 5 nM during 24 hr and 36 hr.* ***C****. Phase contrast images of HEK 293 cells treated with different concentrations and times of the drug where their cell morphology is compared with the untreated control. 5nM PTX was found to induce loss of cytoplasmic processes and cell clusters (arrow). Data reported as mean ± SD and ANOVA with correction for the Tukey test (HSD). Scale bar: 100 µm.*

In contrast, the effect of all tested doses was significant (***p<0.05) at 24 and 36 hr for both cell lines *(Figs 18B and 19B).*

Morphological analysis using phase contrast microscopy, showed no major changes during the first 12 hr of treatment of either cell line due to the cytoplasmic extensions presence that bound to neighboring cells similar to the control *(Figs 18C and 19 C)* and after 36 hr of exposure to the drug, apoptotic vesicles appeared. However, incubation with the drug for 24 hr induced the loss of cytoplasmic processes (arrowheads *in Figs 18C)* and the formation of "cell islands" in the case of HEK 293 cells *(arrow in Fig 87C).* Therefore, the ideal incubation time with PTX for both cell lines was 24 hr at the dose of 5nM.

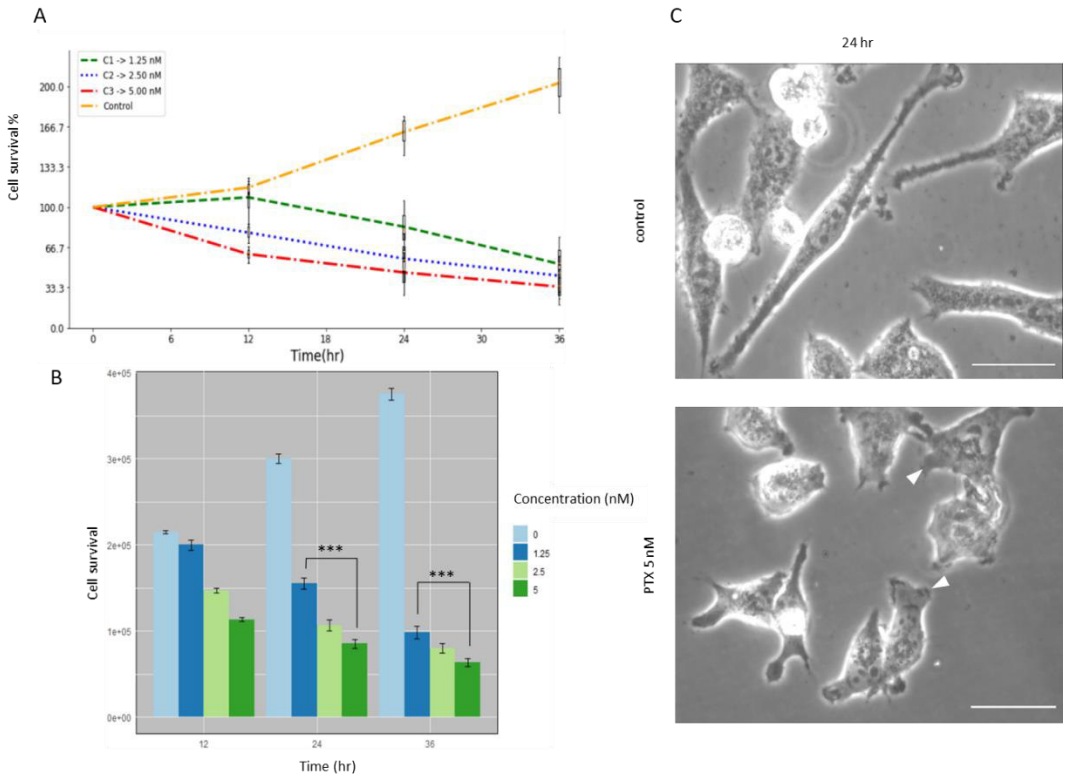

Figure 19. Ideal conditions for treatment with PTX in SHSY5Y cells. A *The curves represent the changes in the percentage of cell survival after treatment with different concentrations of PTX at different times.* ***B*** *Bar graphs, showing a significant decrease (*** P <0.05) in cell survival for PTX 1.25, 2.5 and 5 nM during 24 hr and 36 hr.* ***C****. Phase contrast images of SHSY5Y cells treated with different concentrations and times of the drug where their cell morphology is compared with the untreated control. 5nM PTX was found to induce loss of cytoplasmic processes (arrowheads). Data reported as mean ± SD and ANOVA with correction for the Tukey test (HSD). Scale bar: 100 µm.*

2. Stabilization of microtubules induced by Epo B produced the contraction of cytoplasmic processes in embryonic and neuroblastoma cells at 30nM concentration for 20 hr.

To determine the ideal concentration and time for Epo B treatment, its stabilizer effect on cell proliferation was evaluated. Like in PTX treatment, it was evaluated the changes that Epo B induces on cell survival. Three concentrations of the drug were tested (0.3, 3, 30 nM) at different times (15, 20, 25 hr). The percentage of surviving cells at each concentration and time point was plotted in a linear graph for HEK 293 (Fig 20A) and for SHSY5Y *(Fig. 21A).* it was found that the exposure of both cell lines to the three concentrations of Epo B at all point times was significant (***$p<0.05$), except the concentration of 0.3 nM at 15 hr. *(Figs. 20B and 21B).*

To identify the morphological changes induced by Epo B, the images obtained by PhC microscopy of drug-treated cells and control cells were compared. The exposure of both cell lines to the drug for 15 hr, did not produce important changes, since the cells preserved their cytoplasmic processes like those of the control; however, after 20 hr of incubation with EpoB, the cells exhibited remarkable contraction of their processes *(Figs 20C and 21C)* the effect of "cell islands" was much more evident in HEK 293 cells *(arrow in Fig 20C)*. After 25 hr both cell lines presented apoptotic vesicles that increased with dose dependent manner.

Based on cell survival analysis and the morphological changes observed by PhC microscopy, it was concluded that the ideal concentration and time for Epo B treatment were 30nM for 20 hr.

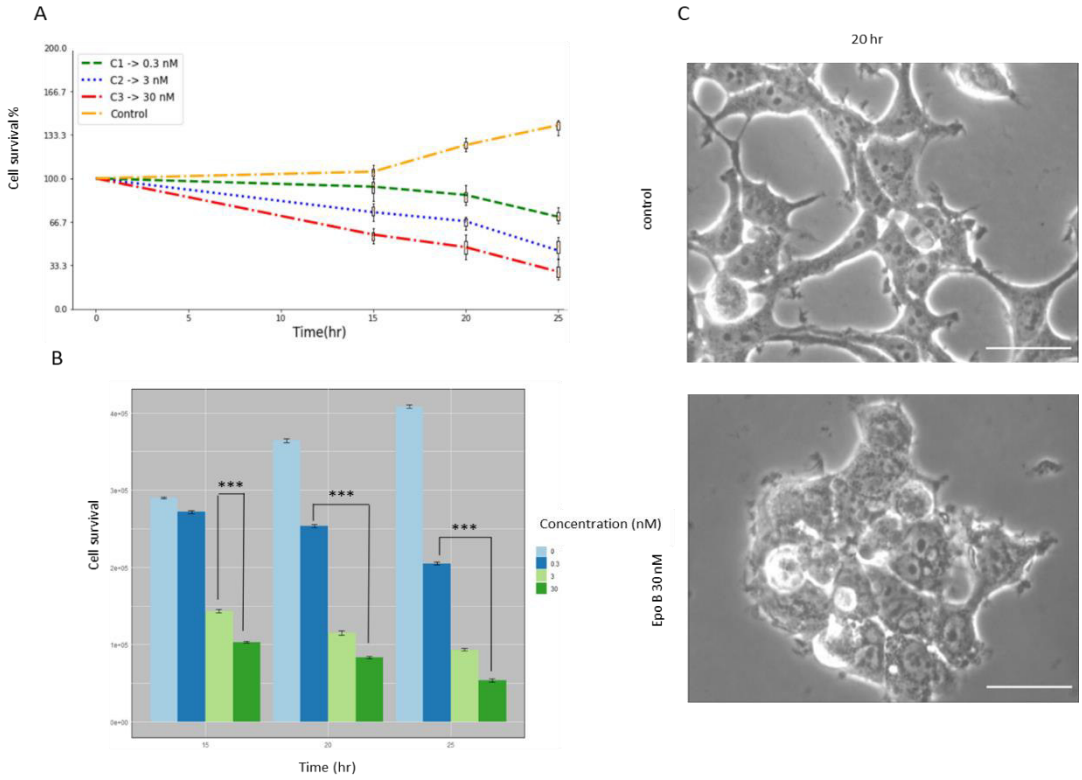

Figure 20. Ideal conditions for treatment with Epo B in HEK 293 cells. A *The curves represent the changes in cell survival after treatment with different concentrations of Epo B at different times. A significant decrease (*** P <0.05) in cell survival was obtained for Epo B 0.3, 3 and 30 nM.* ***B.*** *Bar graphs, showing a significant decrease (*** P <0.05) in cell survival for three concentrations of Epo B during all times.* ***C****. Phase contrast images of HEK 293 cells treated with different concentrations and times of the drug where their cell morphology is compared with the untreated control. Epo B 30nM was found to induce loss of cytoplasmic processes and "island of cells". Scale bar: 100 µm. Data reported as mean ± SD and ANOVA with correction for the Tukey test (HSD).*

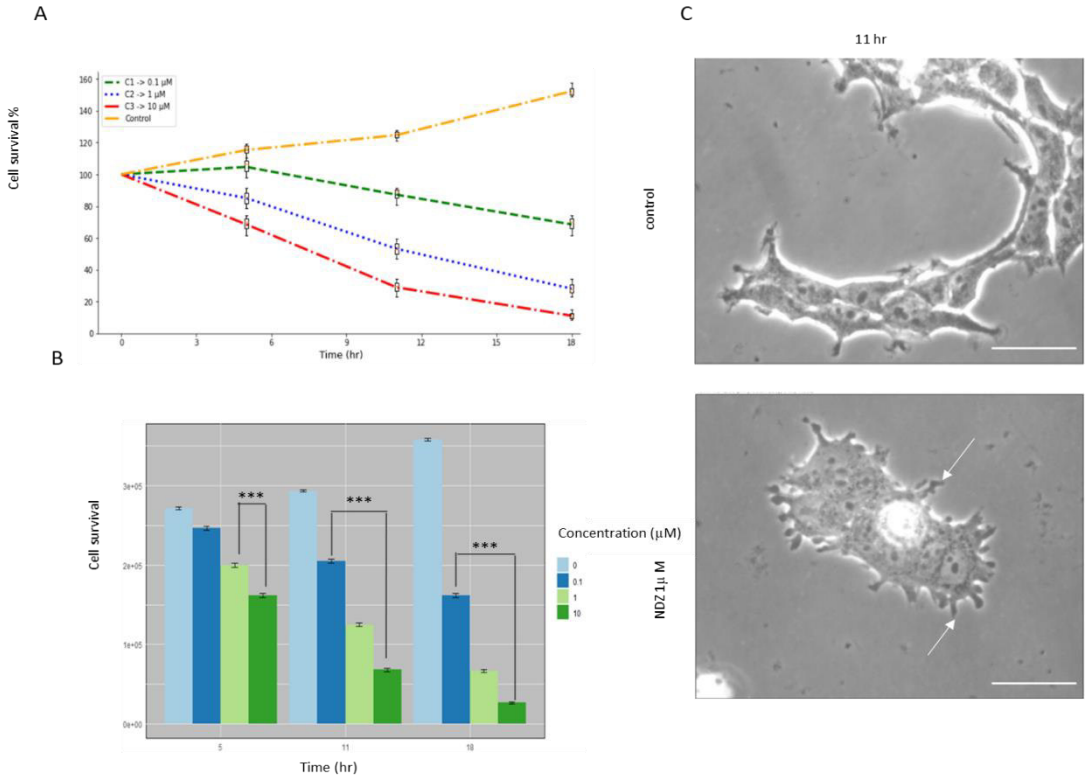

Figure 21. Ideal conditions for treatment with Epo B in SHSY5Y cells. A *The curves represent the changes in cell survival after treatment with different concentrations of Epo B at different times. A significant decrease (*** P <0.05) in cell survival was obtained for Epo B 0.3, 3 and 30 nM.* ***B Bar*** *graphs, showing a significant decrease (*** P <0.05) in cell survival for three concentrations of Epo B during all times.* ***C****. Phase contrast images of SHSY5Y cells treated with different concentrations and times of the drug where their cell morphology is compared with the untreated control. Epo B 30 nM was found to induce remarkable contraction of cytoplasmic processes. Data reported as mean ± SD and ANOVA with correction for the Tukey test (HSD). Scale bar: 100 µm.*

3. Destabilization of microtubules induced by NDZ exhibits the appearance of "protrusions" in the cell membrane in embryonic and neuroblastoma cells at 1µM concentration for 11 hr.

To select the ideal concentration and time for PTX treatment, first the effect of microtubule stabilization on cell proliferation was evaluated. Three different doses of PTX were tested (0.1, 1, 10 µM) at three time points (5, 11, 18 hr). The cellular survival was evaluated by a cell survival assay. The ideal conditions for treatment with NDZ were determined by the analysis of cell survival and morphological changes observed by PhC microscopy. Exposure of both cell lines to NDZ affected cell survival in a dose-dependent manner. Three concentrations of the drug were tested (0.1, 1, 10 µM) at different times (5, 11, 18 hr). The number of surviving cells at each concentration and time point was plotted in a linear graph for HEK 293 *(Fig. 22A)* and for SHSY5Y *(Fig. 23A).* the exposure of both cell lines to the three

concentrations of NDZ at all times point was significant (***p<0.05), except at the concentration of 0.1µM during 5 hr. *(Figs. 22B and 23B).*

The images obtained by phase contrast microscopy showed that the treatment with NDZ, during the first 5 hr, did not present major changes in the morphology of both cell lines compared to the control, however, after 11 hr of exposure to the drug, similar to treatment with Epo B, the cells exhibited a notable loss of their cytoplasmic processes *(Figs 22C and 23C),* in addition, the appearance of "protrusions" in their cell membrane (which is much more evident in HEK 293 cells) *(arrows in Fig 22C).* Many apoptotic vesicles appeared after 18 hr of exposure to NDZ, indicating cell death. These results and those obtained from the analysis of cell survival confirm that the ideal concentration and time for treatment with NDZ were 1µM and 11 hr respectively.

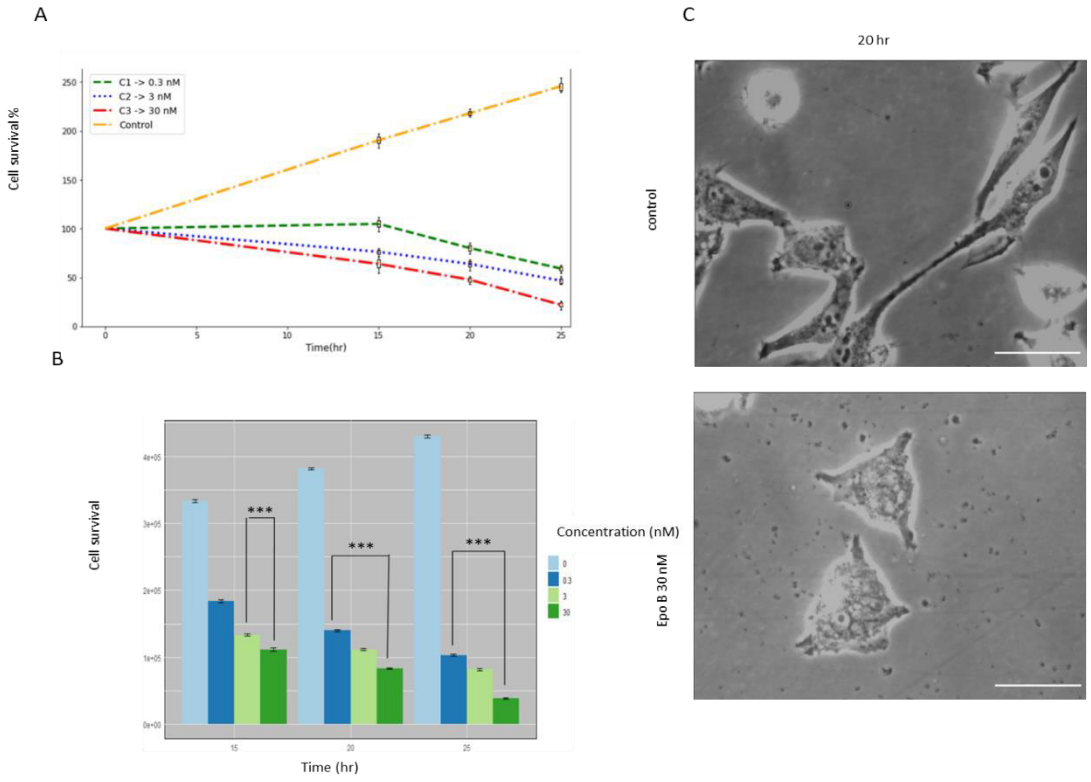

Figure 22. Ideal conditions for treatment with NDZ in HEK 293 cells. A *The curves represent the changes in cell survival after treatment with different concentrations of at different times* ***B.*** *Bar graphs, showing a significant decrease (*** P <0.05) in cell survival for three concentrations of NDZ during all times.* ***C****. Phase contrast images of HEK 293 cells treated with different concentrations and times of the drug where their cell morphology is compared with the untreated control. It was found that NDZ 1 µM induced the formation of "protrusions" in the cell periphery (arrows). Scale bar: 100 µm. Data reported as mean ± SD and ANOVA with correction for the Tukey test (HSD).*

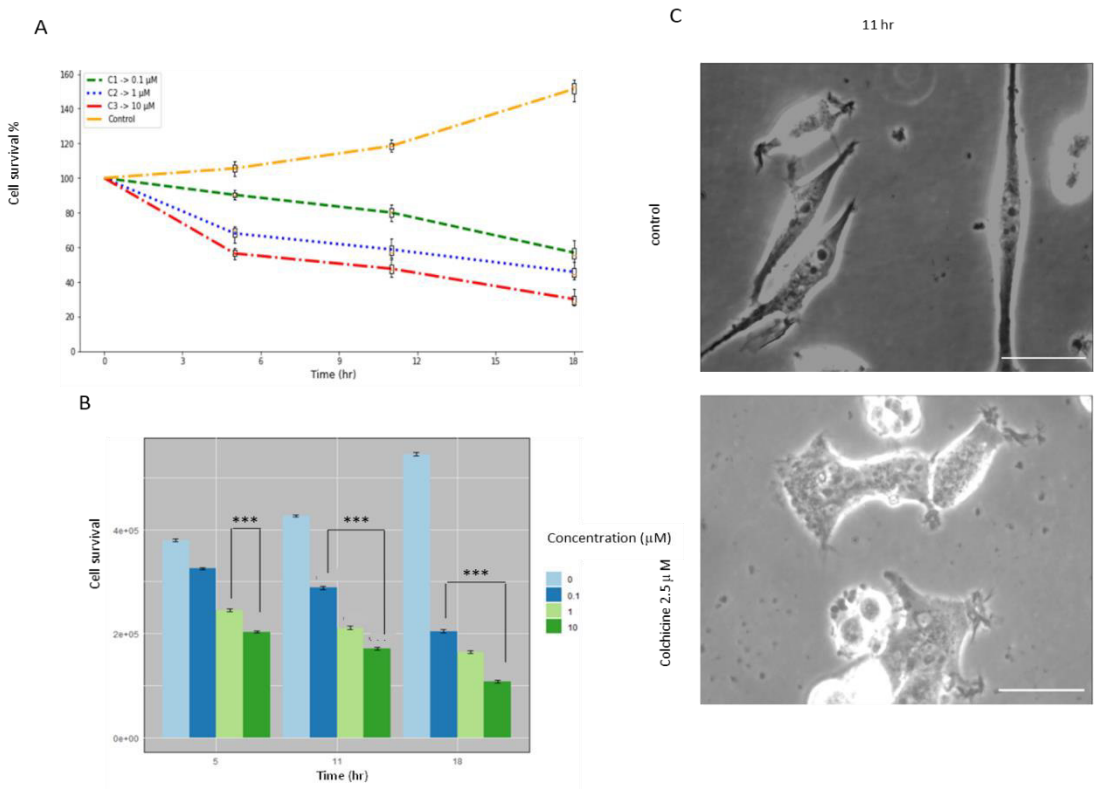

Figure 23. Ideal conditions for treatment with NDZ in SHSY5Y cells. A *The curves represent the changes in cell survival after treatment with different concentrations of NDZ at different times* ***B.*** *Bar graphs, showing a significant decrease (*** P <0.05) in cell survival for three concentrations of NDZ during all times.* ***C****. Phase contrast images of SHSY5Y cells treated with different concentrations and times of the drug where their cell morphology is compared with the untreated control. It was found that NDZ 1 µM produced contraction of cytoplasmic prolongations. Scale bar: 100 µm. Data reported as mean ± SD and ANOVA with correction for the Tukey test (HSD).*

4. Destabilization of microtubules induced by colchicine produce the contraction of cytoplasmatic process in embryonic and neuroblastoma cells at the dose of 2.5 µM during 8 hr.

To select the ideal concentration and time for PTX treatment, first the effect of colchicine on the proliferation rate was evaluated, a cell survival analysis was performed for both cell lines. Three different doses of colchicine were tested (0.23 2.5, 25 µM) at three time points (4, 8, 12 hr). The number of surviving cells at each concentration and time point was plotted in a linear graph for HEK 293 *(Fig. 24A)* and for SHSY5Y *(Fig. 25A).* It was determined that the treatment of both cell lines with the three concentrations of colchicine at all point times was significant (***p<0.05), except for concentration of 0.25 µM at 4 hr *(Figs. 24B and 25B).*

Regarding the morphological analysis, it was found that the exposure of both cell lines to colchicine did not produce important changes in cell morphology during the first 4 hr, however, after 8 hr like the other drugs, contraction of their cytoplasmic processes, loss of contact with neighboring cells and protrusions in the cell membrane (arrows in *Figs 23C and 24C)* were evidenced. In addition, the formation of "cell islands" in the case of HEK 293 cells was maintained *(Figs 24C and 25C)*. Both cell lines presented apoptotic vesicles after 12 hr of drug treatment.

Based on the morphological changes and the survival analysis, it was concluded that the ideal incubation time with colchicine for both cell lines was 8 hr at the dose of 2.5 µM.

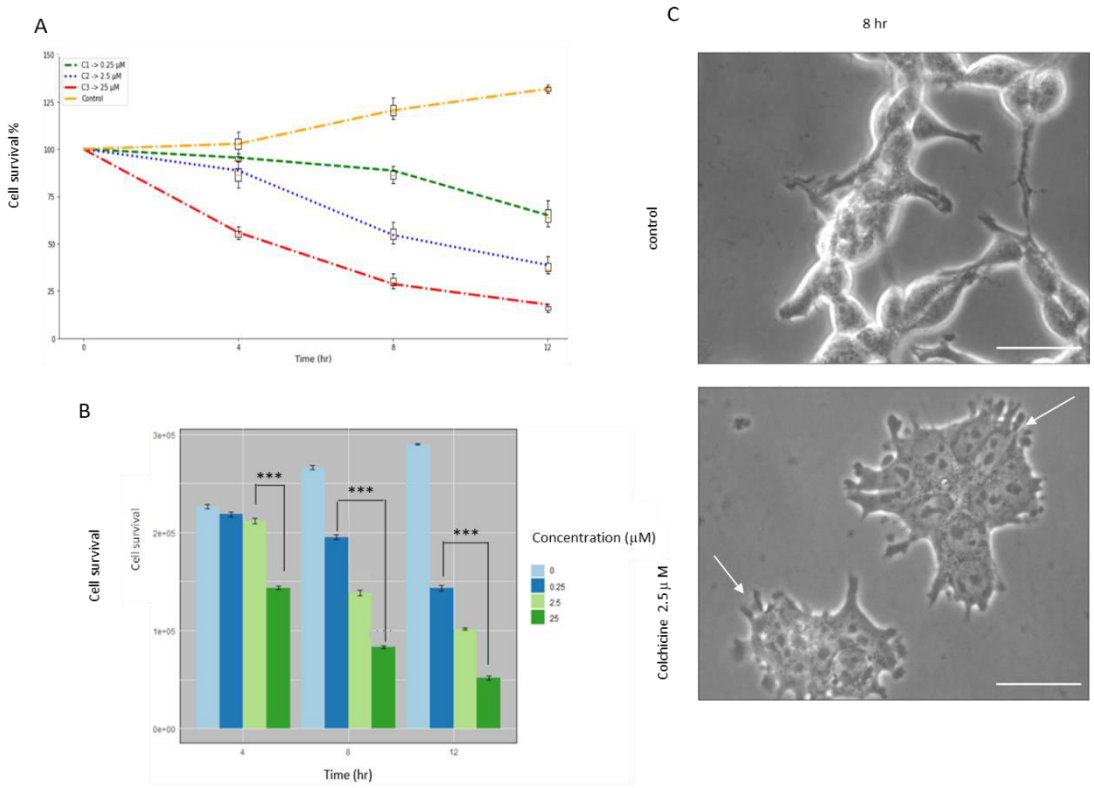

Figure 24. Ideal conditions for treatment with colchicine in HEK 293 cells. A *The curves represent the changes in cell survival after treatment with different concentrations of colchicine at different times* ***B.*** *Bar graphs, showing a significant decrease (*** P <0.05) in cell survival for three concentrations of colchicine during all times.* ***C****. Phase contrast images of HEK 293 cells treated with different concentrations and times of the drug where their cell morphology is compared with the untreated control. Colchicine 2.5 µM was found to induce retraction of cytoplasmic prolongations and* protrusions on the cellular periphery *(arrows). Scale bar: 100 µm. Data reported as mean ± SD and ANOVA with correction for the Tukey test (HSD).*

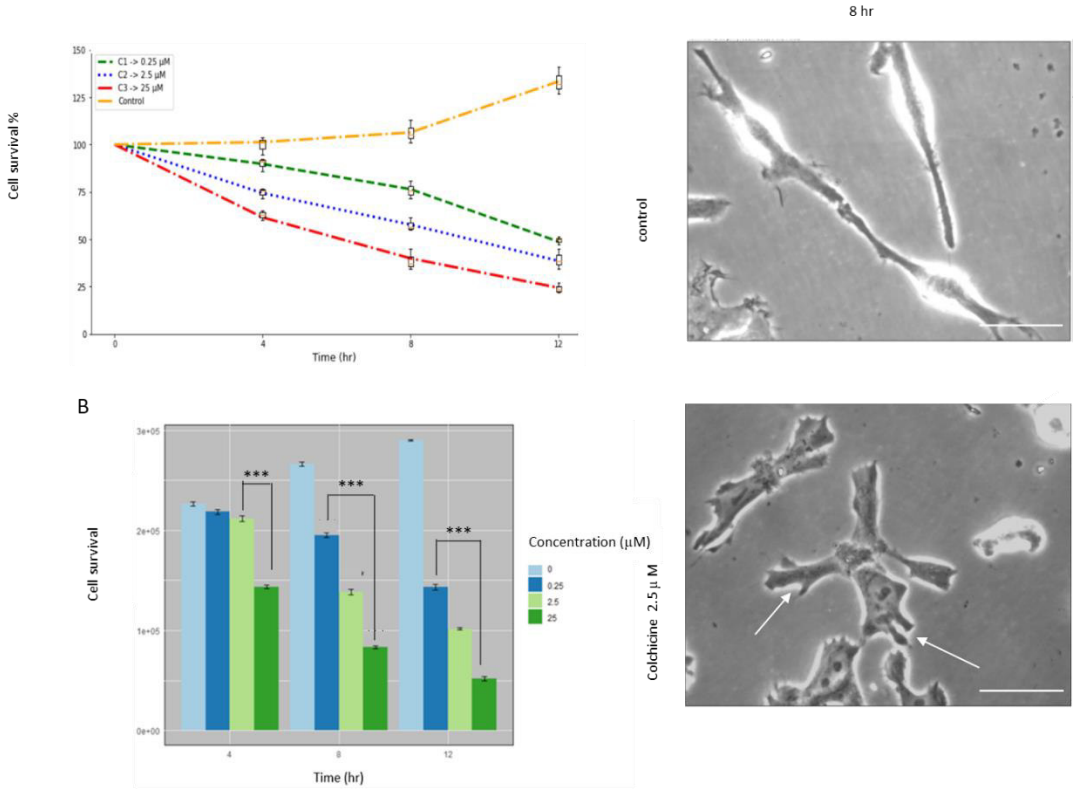

Figure 25. Ideal conditions for treatment with colchicine in SHSY5Y cells. A *The curves represent the changes in cell survival after treatment with different concentrations of colchicine at different times* ***B.*** *Bar graphs, showing a significant decrease (*** P <0.05) in cell survival for three concentrations of colchicine during all times.* ***C*** *Phase contrast images of SHSY5Y cells treated with different concentrations and times of the drug where their cell morphology is compared with the untreated control. Colchicine 2.5 µM was found to induce retraction of cytoplasmic prolongations and* protrusions on the cellular periphery *(arrows). Scale bar: 100 µm. Data reported as mean ± SD and ANOVA with correction for the Tukey test (HSD).*

The concentration and time selected for each drug are shown in the following table *(table 3.).* Subsequently, fluorescence immunohistochemistry was performed for tubulin, in order to identify by means of confocal microscopy, the structural changes in the cultures treated with the drugs.

	Drugs			
Concentration	paclitaxel	epothilone B	nocodazole	colchicine
	5nM	30 nM	1 µM	2.5 µM
Incubation time (hr)	24	20	11	8

Table 3. Concentration and time selected for each drug.

Results

1. Treatment with PTX and Epo B induces higher tubulin density.

1.1 Cells treated with PTX 5nM.

In the cell, PTX acts as stabilizer of tubulin dimers inhibiting the MTs depolymerization. Since in H-ABC-tubulinopathy, the accumulation of MTs around the endoplasmic reticulum was described, these drugs, which affect microtubule dynamics were used to understand the defect in MTs that occurs in the disease. Fluorescence images of HEK 293 cells treated with PTX 5nM were consistent with PhC microscopy images *(Fig 18C),* in which the formation of "cell islands" with very short cytoplasmic extensions was evident *(Figs 26 B-B' and C-C').* The fluorescent tubulin labeling is homogeneous in the control *(Figs 26 A and A')*, while tubulin in the cells treated with PTX is concentrated mainly in the periphery of the "cell islands" with the nuclei located in the center *(Figs 26 B and C).* This effect is seen in greater detail in the *Figs 26 B' and 26 C',* where only the tubulin labeling is shown. It was also observed a greater fluorescence intensity of the marker in this area, suggesting a greater tubulin density. This assumption was corroborated by fluorescence density analysis, where the density was defined as the intensity divided by the number of pixels in the region of interest (ROI), it was found that cells exposed to PTX 5nM exhibited a significant increase (*** $p < 0.05$, one-way ANOVA with Tukey's test correction (HSD)) in fluorescence density compared to the untreated control.

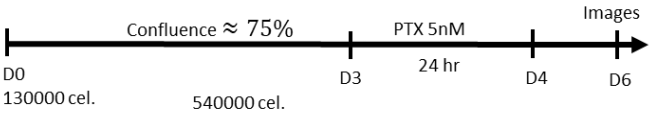

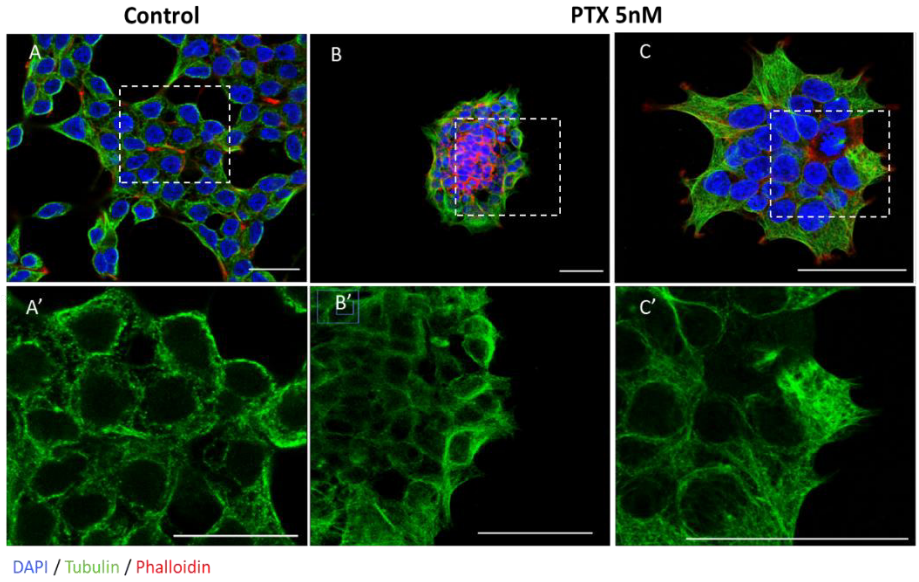

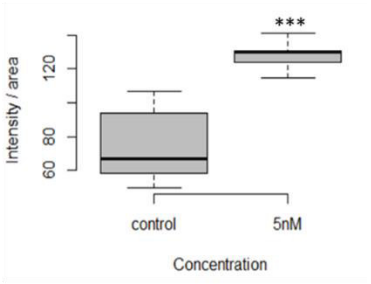

Figure 26. PTX 5nM induced accumulation of tubulin in the periphery of HEK 293 cells *Confocal immunofluorescence images of tubulin (green), nucleus (blue), and actin (red). In HEK 293 cells treated with PTX, a higher density of tubulin fluorescent label is observed in the cell periphery (B-B' and C-C'F), compared to the control (A and A'). Scale: 50 µm. Cells treated with PTX exhibit higher tubulin density. The graph represents the fluorescence density (intensity / number of pixels) of tubulin in HEK 293 cells treated with paclitaxel 5nM. The treated cells show a fluorescence density significantly higher than the untreated controls (*** p <0.05); One-way ANOVA with Tukey's test correction (HSD). Scale bar: 50 µm*

1.2 Cells treated with Epo B 30nM.

Like PTX, epothilone B is a microtubule stabilizer, thus promoting their polymerization. In confocal images, it was observed that Epo B induced contraction of cytoplasmic processes and association of cells in clusters (*Figs 27 B-B' and C-C').* Unlike the control condition, where tubulin extends radially from the MTOC *(Figs 27 B-B' and C-C').,* in cells treated with Epo B tubulin distributes in the cell periphery, oriented in parallel bundles radiating out from the nucleus (*Figs 27 B-B' and C-C').* The areas where tubulin is more concentrated also showed a higher intensity of fluorescent labeling for tubulin, which was correlated with a significant increase in fluorescence density (*** p <0.05), using One-way ANOVA with Tukey's test correction (HSD).

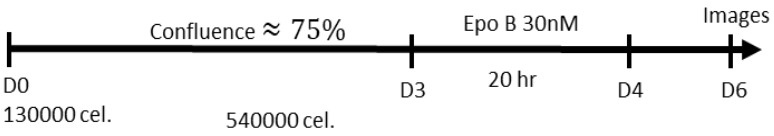

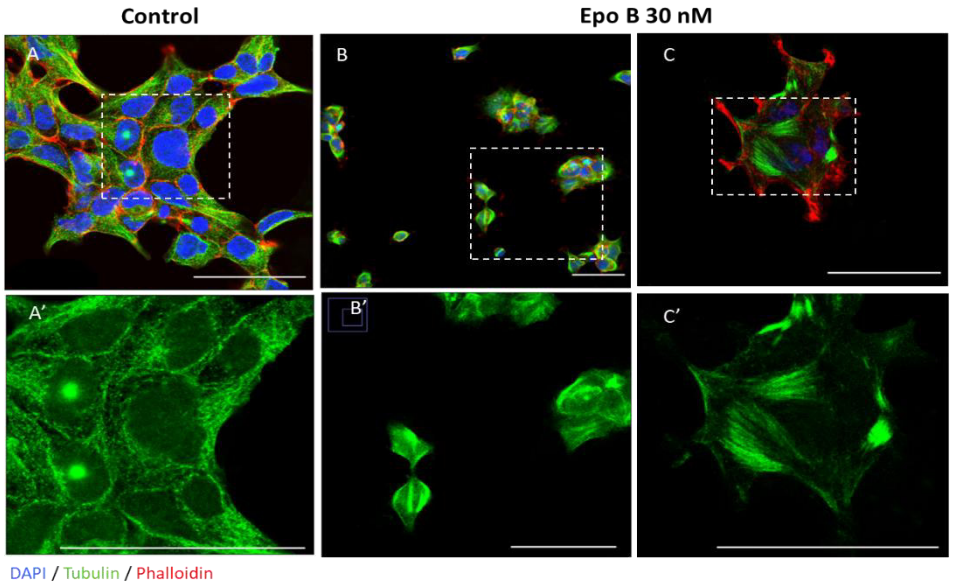

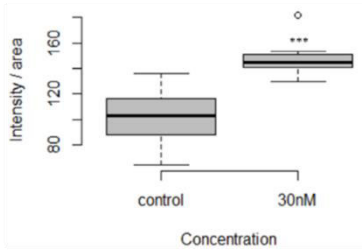

Figure 27. Epo B 30nM produced bundles of tubulin in HEK 293 cells. *Confocal immunofluorescence images of tubulin (green), nucleus (blue), and actin (red). In HEK 293 cells treated with Epo B, a mayor fluorescent label is observed in the cell periphery (B-B' and C-C'), compared to the control (A and A'). Cells treated with Epo B show higher tubulin density. The graph represents the fluorescence density (intensity / number of pixels) of tubulin in HEK 293 cells treated with epothilone B 30 nM. The treated cells show a fluorescence density significantly higher (*** p <0.05) than the untreated controls); One-way ANOVA with Tukey's test correction (HSD). Scale: 50 µm.*

This result suggests that the increase in tubulin density, induced by treatment with PTX and Epo B could be related to the microtubular defect observed in OLGs with the mutation in TUBB4A, due to the abnormal abundance of MTs.

1.3 Cells treated with NDZ 1 µM.

Nocodazole acts as a microtubule destabilizer, which binds to β tubulin, promoting its depolymerization. Since it affects microtubule dynamics, it was used to study the molecular mechanisms that could produce the microtubule defect in H-ABC. Fluorescence images of HEK 293 cells exposed to 1 µM NDZ show, like the other drugs, contraction of cytoplasmic processes and clustering of cells *(Figs 28 B-B' and C-C')* compared to the control. Particularly, with this drug, protrusions are observed in the membrane, which, as observed in the tubulin images *(Figs 28 B-B' and C-C')* appeared as small punctate aggregates in the

cell periphery, suggesting that they could be abnormal spindles, as a product of the mitotic arrest, according to previous studies with this drug [51].

Furthermore, the fluorescent signal of tubulin appears slightly weak and diffuse in the cytoplasm of the cells treated with NDZ *(Figs 28 B-B' and C-C')* compared to the control, where a homogeneous labeling is observed throughout the cell (*Figs 28 A and A').*

On the other hand, the fluorescence density analysis showed that there is no significant change (ns) between the cells treated with the drug and the control condition, thus suggesting that the aggregates of tubulin in the periphery could "compensate" for the weak signal, which is observed in the cell cytoplasm.

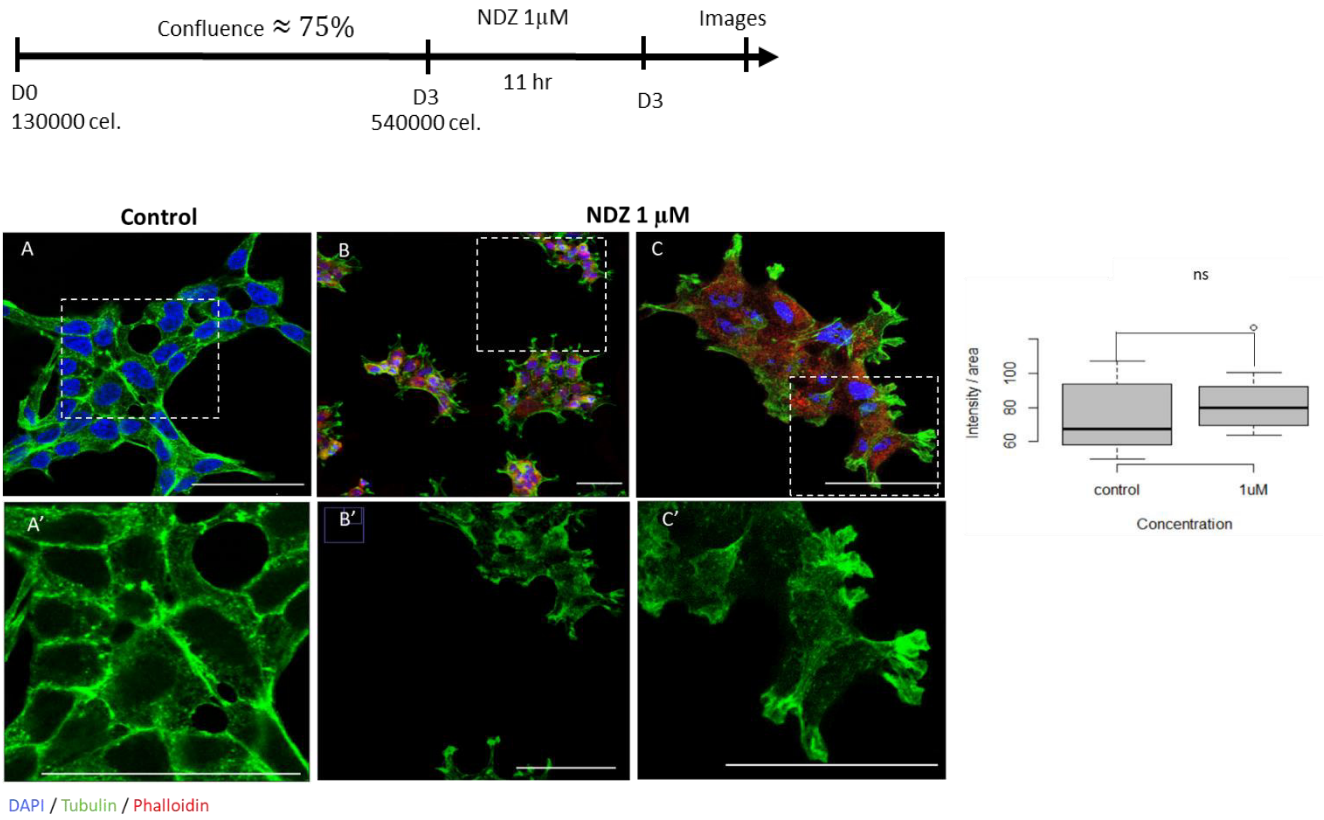

Figure 28. NDZ 1µM induces depolymerization of MTs with the formation of tubulin aggregates in the cellular periphery*. Confocal immunofluorescence images of tubulin (green), nucleus (blue), and actin (red). In HEK 293 cells treated with NDZ 1µM, aggregates of tubulin are observed in the cell periphery (arrows) (B-B' and C-C'), compared to the control (A and A'). Scale: 50 µm. Fluorescence density (intensity / number of pixels) of tubulin in HEK 293 cells treated with NDZ 1µM.The treated cells did not show significant changes (ns) in fluorescence density compared to the untreated control; One-way ANOVA with Tukey's test correction (HSD).*

1.4 Cells treated with colchicine 2.5µM.

Colchicine inhibits the assembly of MTs, affecting their stability, however, at high concentrations (such as those used in this work), it induces the catastrophe of MTs. The exposure of HEK 293 cells to 2.5 µM colchicine produced a weaker tubulin signal *(Figs 29 B-B' and C-C'),* than the treatment with NDZ *(Figs 28 B-B' and C-C'),* the tubulin labeling in the treated cells is not clearly appreciated *(Figs 29 B-B' and C-C'),* compared to the control *(Figs 29A and A'),* which suggests an almost complete disruption of the microtubule network, possibly due to depolymerization. [55]. This effect is correlated with the diffuse signal of tubulin, observed in the *Figs 29 B' and C'.* The data obtained with fluorescence density analysis confirm this result, since the cells treated with colchicine exhibited a significant (*p <0.05) decrease in tubulin density compared to the control.

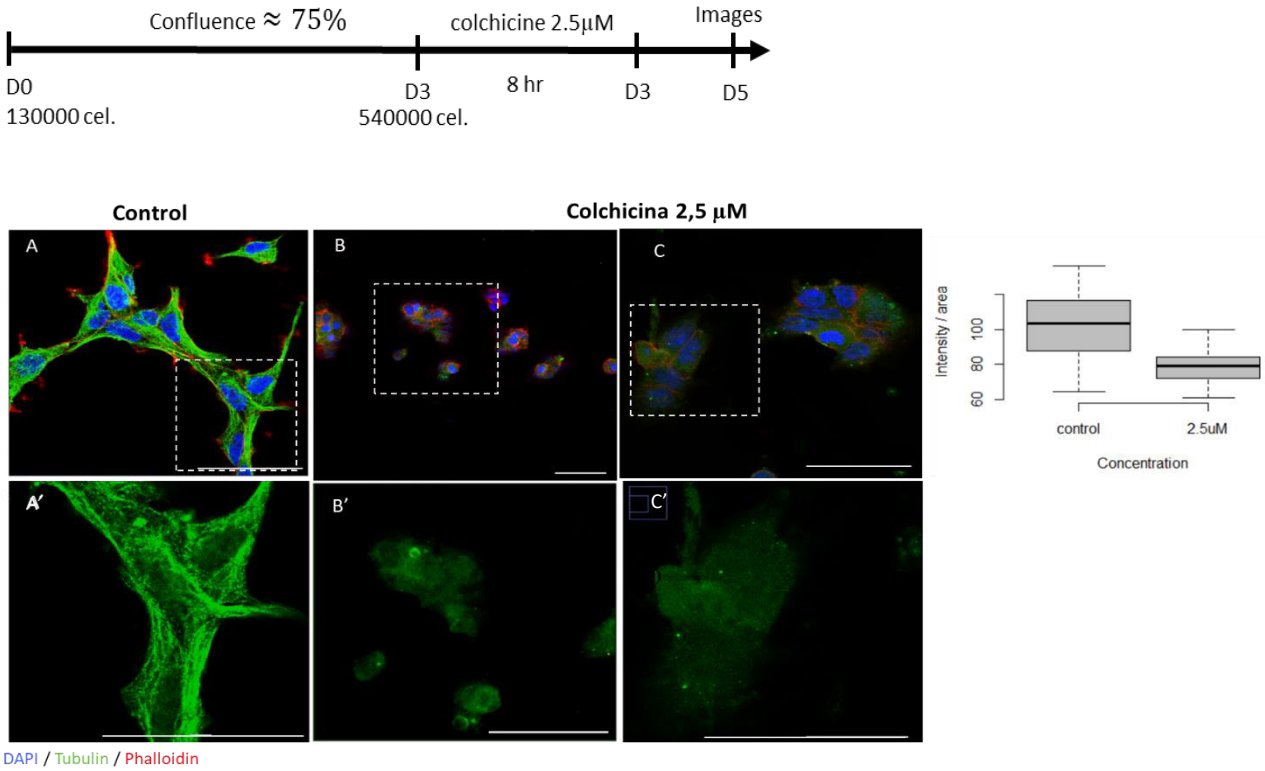

Figure 29. Colchicine 2.5µM produced a disruption in tubulin lattice*. Confocal immunofluorescence images of tubulin (green), nucleus (blue), and actin (red). In HEK 293 cells treated with Colchicine 2.5µM a very weak and diffuse signal of the tubulin labeling is observed (B-B' and C-C'), compared to the control (A and A'). Scale: 50 µm. G The graph represents the fluorescence density (intensity / number of pixels) of tubulin in HEK 293 cells treated with Colchicine 2. 5µM. The treated cells showed a lower fluorescence density compared to the untreated controls (*p <0.05) One-way ANOVA with Tukey's test correction (HSD).*

2. The corpus callosum of *taiep* rat show a higher tubulin density than WT.

The corpus callosum is a group of nerve fibers that connects the cerebral hemispheres, and its main function is to maintain interhemispheric communication. This structure is formed mainly by myelinated axons, so it is to be expected to find many OLs there.

Coronal slice images of the 9-month-old taiep rat brain showed a higher number of cells in the corpus callosum, probably OLs, which exhibit more intense tubulin signal *(Figures 30 B and B')* compared to the wild type (WT) rat *(Figures 30 A-A')*. This observation can be related with the previously described abnormal abundance of MTs in the OLs of the *taiep* rat, which persisted up to two years of age [6], [7].

The areas where tubulin labeling is more intense also showed a significant increase in fluorescence density (** p <0.05, using One-way ANOVA with Tukey's test correction (HSD) *(Fig 30 C).*

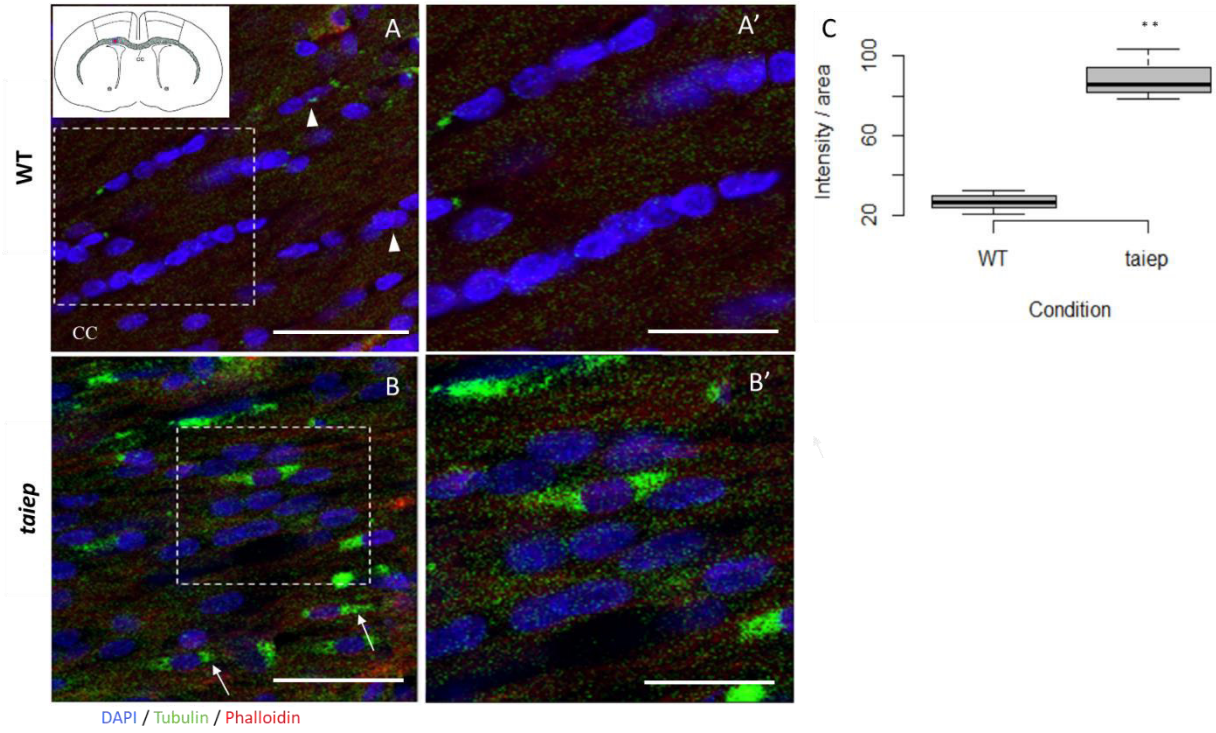

Figure 30. The corpus callosum (CC) of the taiep rat exhibits higher tubulin density. *Confocal immunofluorescence images of tubulin (green), nucleus (blue), and actin (red). In the taiep rat it is observed that the fluorescent labeling of tubulin is more intense (arrows) (Figs A and A') compared to the WT rat (arrowheads) (Figs B and B').*

3. The effect of paclitaxel and epothilone B depends on the differentiation phase of SHSY5Y cells.

To investigate the effect of PTX and Epo B on the differentiation process, undifferentiated SHSY5Y cells were compared with SHSY5Y cells in phase of differentiation, exposed to 20 μM retinoic acid for 4 days.

It was found that the treatment of undifferentiated SHSY5Y cells with PTX 5nM and Epo B induced multinucleation, since the cells contained evenly stained nuclear fragments, as well as abnormal spindles *(Figs 31 B-B', C-C')* (arrows), possibly because of a mitotic arrest in the metaphase, which these MTA usually cause.

Regarding their morphology, the treated cells are completely contracted (*Figs 31 B-B', C-C'),* compared to the control, where tubulin (in green) is observed fully distributed in the cytoplasm, with actin filaments in the periphery and a condensed core *(Figs 31 A-A').*

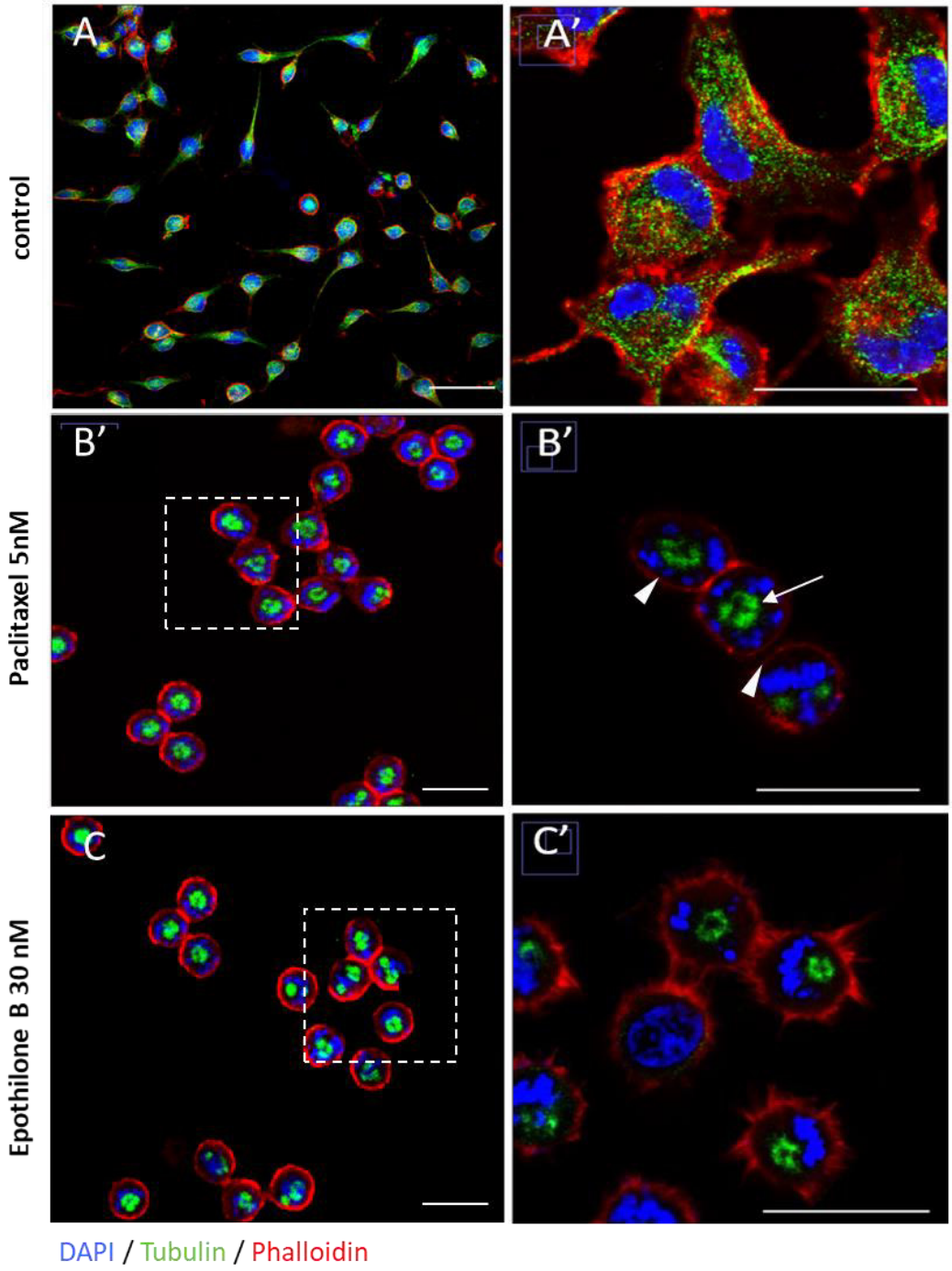

Figure 31. PTX 5nM and Epo B 30nM induce multinucleation and abnormal spindle formation. *Confocal immunofluorescence images of tubulin (green), nucleus (blue), and actin (red). SHSY5Y cells treated with PTX5 nM and Epo B 30 nM exhibit multipolar spindles (arrow) with chromosomes close to their poles (arrowheads) (B-B' and C-C'), an effect not observed in the control no treated (A and A'). Scale: 50 µm.*

The exposure of SHSY5Y cells to retinoic acid induces their differentiation, since it promotes the expression of adrenergic receptors, in addition to changes in their morphology, as an extension of their processes and neurite development [56];[57].

Cells were treated with retinoic acid as indicated in the following timeline:

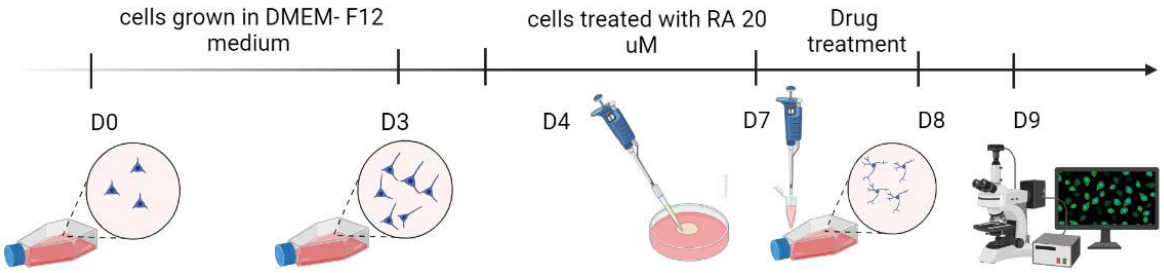

The fluorescence images of SHSY5Y cells treated during four days with retinoic acid, showed prolongations and neurites *(Figs 32 A and B),* compared to the untreated ones *(Figs 31 A-A'),* as reported in previous studies*.* Cells in differentiation phase were then exposed to Epo B 30 nM for 20 hr and the changes in their cytoskeleton were analyzed. It was found that the cells treated with Epo B could be classified into two groups: the first one corresponded to cells with quite extensive processes *(Figs 32 C and D) (arrows)* and the second one consisted of cells with almost complete contraction of their processes *(Figs 32 C and D, arrowheads)*. These results suggesting that the effect of contraction of the processes and the fragmentation of the nucleus could correspond to undifferentiated SHSY5Y cells *(Fig 31 C and C '),* however, the maintenance of extensive prolongations in another group of cells could be since Epo B is a microtubule stabilizer, which could be favoring polymerization in this type of cells [58].

Another group of cells treated with retinoic acid were exposed to PTX 5nM for 24 hr. In the fluorescence images, it is observed that, unlike Epo B treatment, most of them exhibit extended prolongations *(Figs 32 E and F),* similar to those of the control *(Figs 32 A and B),* however they appeared to have longer neurites *(Figs 32 E and F) (arrows)* compared to the control *(Figs 32 A and B),* suggesting that MTs might still be dynamic in the differentiation phase of SHSY5Y and that stabilization of microtubule induced by PTX contributes to the lengthening of neurites.

These findings together suggest that PTX and Epo B act differently according to the differentiation phase of the SHSY5Y cells, since it was found that both drugs induced multinucleation in an undifferentiated stage *(Figs 31 B-B' and C-C')* while, after treatment with retinoic acid, the drugs seem to stabilize and elongate the processes of the cells, being much more evident in the treatment with PTX.

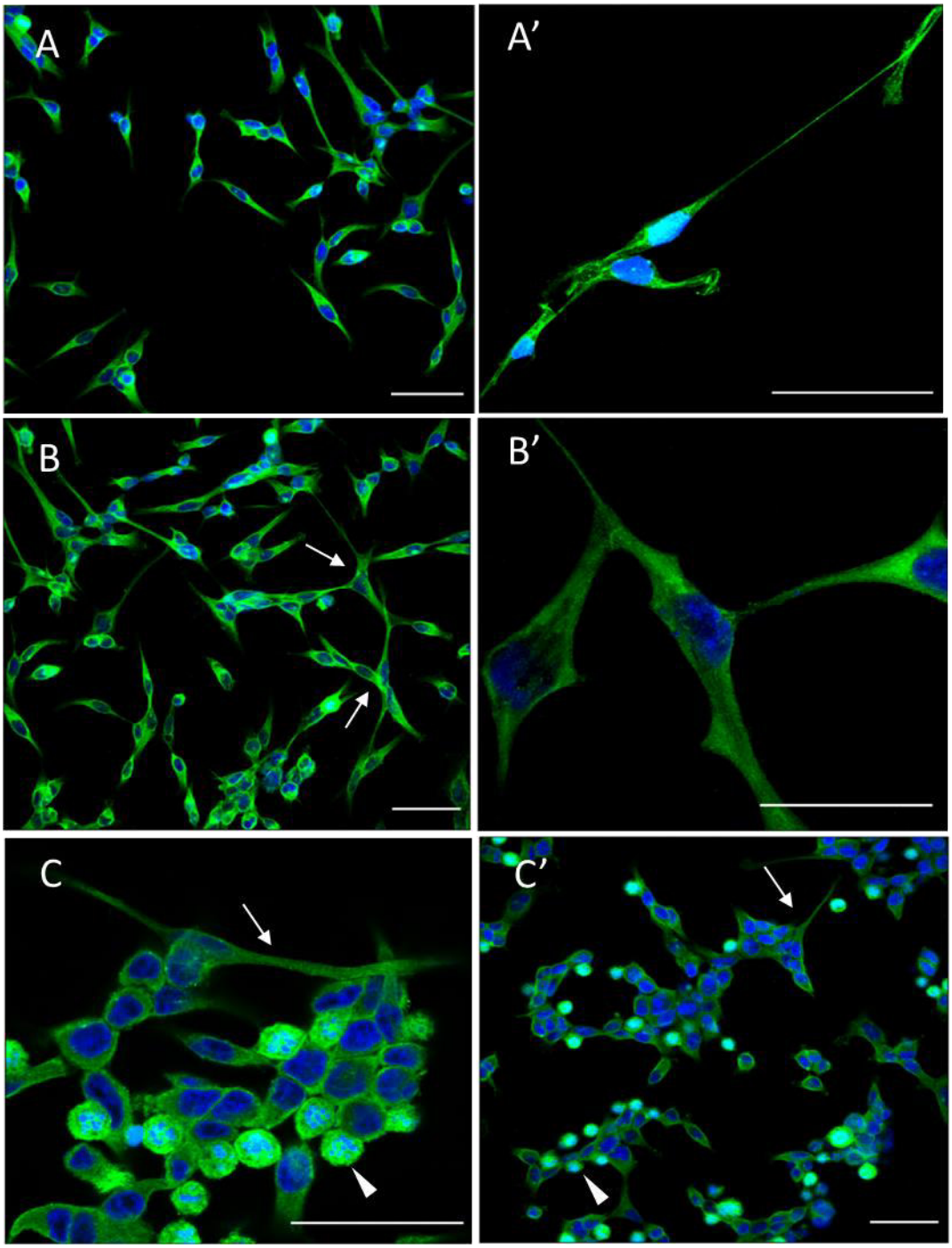

Figure 32. PTX 5nM and Epo B 30nM induce extension of process in differentiated SHSY5Y cells*. Confocal immunofluorescence images of cells treated with AR/Epo B 30 nM (C and D) and AR/PTX 5nM (E and F). Arrowheads: Contraction of prolongations an multinucleation; Arrows: Extension of processes; Neurites of extensions. Tubulin (green), nucleus (blue). Scale: 50 µm.*

Discussion

In this work we identify the effect of specific drugs on the cytoskeleton of two human cell lines, in order to develop a pharmacological model that allows to understand the pathophysiological processes that trigger hypo-demyelination and central malformations characteristic of H-ABC.

We demonstrated that treatment with PTX and Epo B induces a higher tubulin density. This result could be related to the changes produced by the mutation in H-ABC, since there is an abnormal abundance of microtubules [59]; [6], suggesting that these drugs can be used as pharmacological tools to study the structural modifications that occur in the cytoskeleton of patients with H-ABC. Furthermore, it was observed that in the *taiep* rat, the cells in the corpus callosum present more intense tubulin labeling than in the WT rat. Knowing that corpus callosum is composed principally by OL [78] this finding suggests that the cells accumulating tubulin in their cytoplasm corresponds to OLs. This finding is consistent with previous studies, in which the accumulation of MTs in H-ABC as a consequence of mutation is reported [6]; [7];[60].

H-ABC is a tubulinopathy produced by mutations in TUBB4A [2]. Our laboratory has identified the *taiep* rat as the first animal model of tubulinopathies [61]. Both in humans and in the *taiep* rat, it has been shown that they present severe damage in the central myelin and atrophy in the corpus callosum and cerebellum [61]. At the cellular level, the patient and *taiep* rat have an excess of MTs organized in longitudinal arrays, many of which are closely related to the profiles of the smooth endoplasmic reticulum [6], [7]. These microtubular defect could interfere with transport from endoplasmic reticulum to the Cis portion of the Golgi apparatus [62], affecting the components necessary for forming and maintaining the myelin sheath [63].

Diverse intrinsic factors influence microtubule dynamic: tubulin isotype, post-translational modifications, and its interaction with different microtubule-associated proteins (MAPs) [64]. For example, the assembly of neuronal MTs is slower than in glial cells because they are in contact with MAP 2 or tau [65]. Likewise, detyrosination promotes the state of polymerization of the microtubule [66], and it is used as a marker of stable MTs. The post-translational modifications can also influence the localization of microtubule-associated proteins. Plus end-tracking proteins (+TIPs) accomplish important functions for MTs, such as regulating their dynamics by acting as an anti-catastrophe factor [67].

A possible explanation to the different effects obtained with the treatment of PTX and Epo B in cell cultures, could be the isotype of tubulin that they express. For example, HEK 293 cells express TUBA1A, TUBA1B, TUBB2, TUBB4, and TUBB5 [68], while SHSY5Y cells express TUBB1, TUBB2, TUBB3[69] and TUBB4A [70]. It has been reported that MTs assembled from TUBB2 and TUBB4 are less dynamic than those assembled from TUBB3, due to the fact that

they nucleate slower and exhibit a lower catastrophe rate [64]. This could be related to resistance to PTX. In previous studies, it was shown that the overexpression of TUBB2 and TUBB4 results in resistance to PTX and its stabilizing effect on MTs, as it is the case of MCF-7 cells. However, the results reported in this work suggest high sensitivity of HEK 293 and SHSY5Y cells to this drug, possibly because they do not exhibit overexpression of these tubulin isotypes. Furthermore, it is possible that in the case of HEK 293 cells, PTX and Epo B stabilizes the microtubules of the cell periphery (which are generally more dynamic*, Figs 29 and 31)*, this hypothesis could be related to the fluorescence images in which a more intense tubulin labeling is observed, correlated with the significant increase in fluorescence density in image analysis *(Figs 30 and 32).* On the other hand, in the case of undifferentiated SHSY5Y cells, multinucleation and abnormal spindle formation with chromosomes outside the metaphase plate is quite evident with PTX and Epo B treatment *(Fig 38 B-C'),* suggesting their sensitivity to these drugs. However, the cells treated with retinoic acid, which were in a differentiation phase, showed a different effect to PTX and Epo B, i.e., they had longer prolongations and the appearance of neurites *(Fig 39 E and F).* These results are consistent with previous studies, which indicate that during neuronal differentiation the expression of TUBB3A increases [69], which is also related to resistance to taxanes probably because the MTs formed from this kind of tubulin are more dynamic [64]. Interestingly, differentiated SHSY5Y cells treated with PTX were not significantly affected; they even exhibited longer neurites (Figs C- C'). This result is consistent with that reported by Park and his collaborators, suggesting that the differentiated neurons still present a population of dynamic microtubules, which PTX stabilizes [77].

Based on these findings, it is possible that the microtubular defect observed in the oligodendrocytes of H-ABC is that their dynamics changes. Electron microscopy images show MTs aligned around the endoplasmic reticulum with their membranes joined [7]. A hypothesis to this is that it is the result of an alteration in dynamic instability, it is possible that the microtubules are not depolymerizing adequately, or a defect in polymerization is occurring, given the abnormal abundance of MTs. However, there is also a higher number of them [7]; [59], suggesting an alteration in the synthesis of tubulin. *In vitro* studies show that PTX slightly increases the rate of tubulin synthesis [71]. Furthermore, it has been described that PTX induces a notable increase in cytoplasmic MTs in OLs in CNS organotypic cultures [72], a pattern almost identical to that observed in OLs of the *taiep* rat. Thus, PTX in CNS organotypic cultures model could provide insights about the changes in the microtubules observed in the *taiep* rat.

The microtubule abnormalities in OLs observed in patients and the *taiep* rat, are responsible for the reduced membrane sheets and decreased levels of myelin proteins [59]. Previous experiments demonstrated that NDZ treatment allowed the correct distribution of PLP in OLs in the spinal cord of the *taiep* rat [58], pointing out a possible alteration in microtubule dynamics that affect myelin synthesis in OLs.

In conclusion, these results suggest that treatment with drugs that affect the microtubular dynamics will be a helpful tool to study the structural modifications that occur in the cytoskeleton of patients with H-ABC.

More experiments are required to confirm that the increase in tubulin density observed with PTX, and Epo B treatment corresponds to polymerized MTs. In turn, experiments with molecular modeling that would allow understanding whether the effect on MTs induced by these drugs is related to the microtubular defect observed in OLs with H-ABC.

Similarly, performing these experiments with OLs suggests a good mechanism to describe the pathological processes that occur in the cytoskeleton of patients with H-ABC.

Conclusions

- PTX and Epo B induce higher tubulin density, an effect similar to that described in OLs with the TUBB4A mutation. Therefore, the microtubular defect of the OLs could be the product, among other aspects, of an alteration in the dynamics of the MTs.

- High concentrations of NDZ and colchicine induce a disruption of the microtubule network suggesting depolymerization.

- Treatment of SH-SY5Y cells with PTX and Epo B resulted in the formation of abnormal spindles and a multinucleated effect, indicating that these drugs have a range of results depending on the type of tubulin isoform that the cells express.

- The corpus callosum of the *taiep* rat exhibits a higher number of OLs with a more intense fluorescent tubulin labeling compared to WT, which could suggest a higher density of MTs; however, more experiments are required to confirm this.

- The use of drugs that affect microtubule dynamics can be a helpful tool to study the structural modifications in the cytoskeleton of patients with H-ABC.

Annexes

Annex 1. Tukey's test for the treatment of HEK 293 cells with PTX.

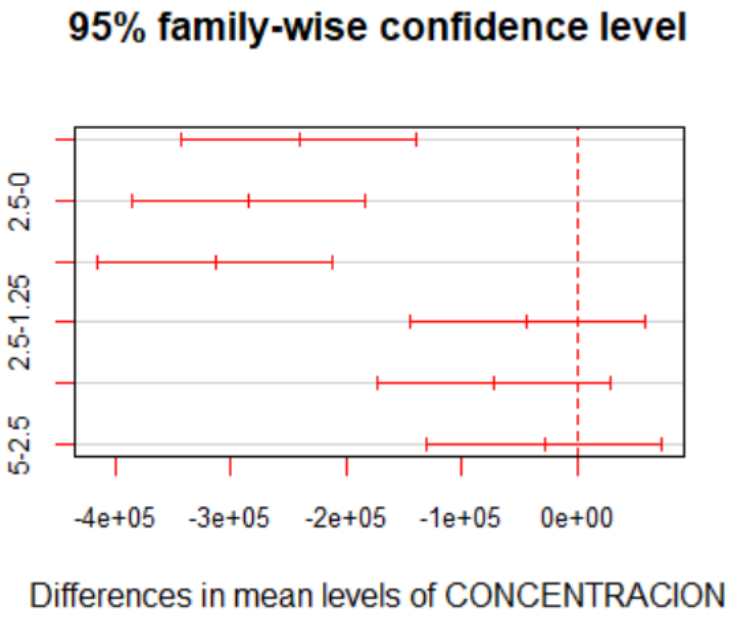

Annex 2. Tukey's test for the treatment of SH-SY5Y cells with PTX.

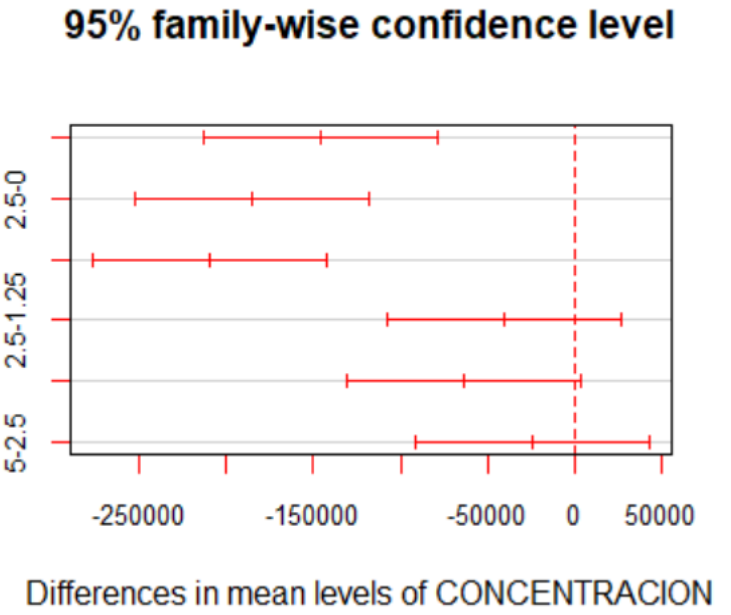

Annex 3. Tukey's test for the treatment of HEK 293 cells with Epo B.

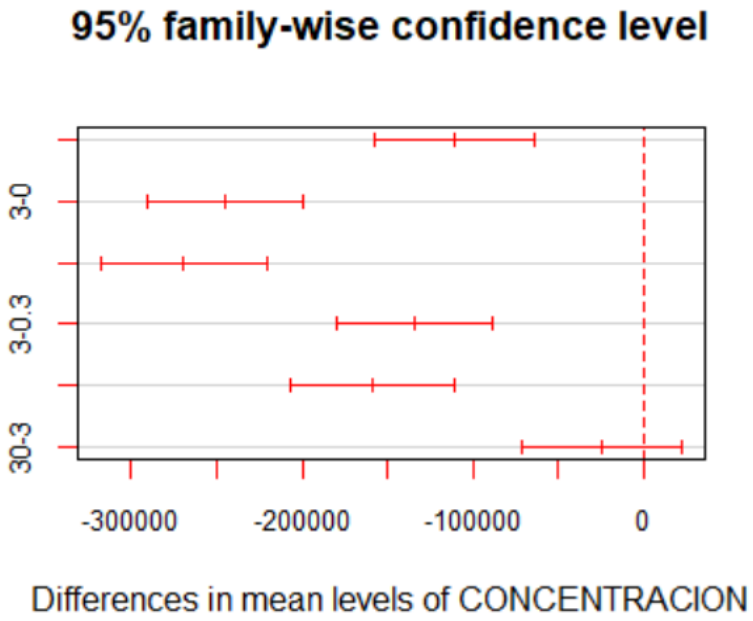

Annex 4. Tukey's test for the treatment of SHSY5Y cells with Epo B.

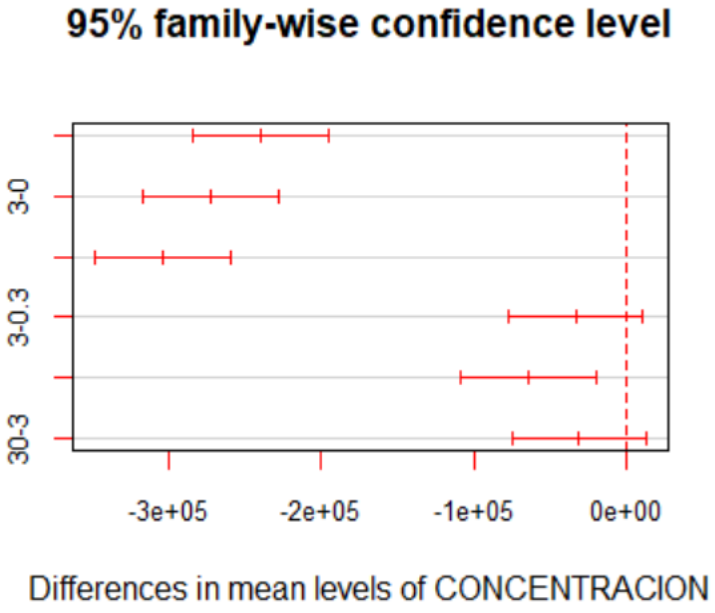

Annex 5. Tukey's test for the treatment of HEK 293 cells with NDZ

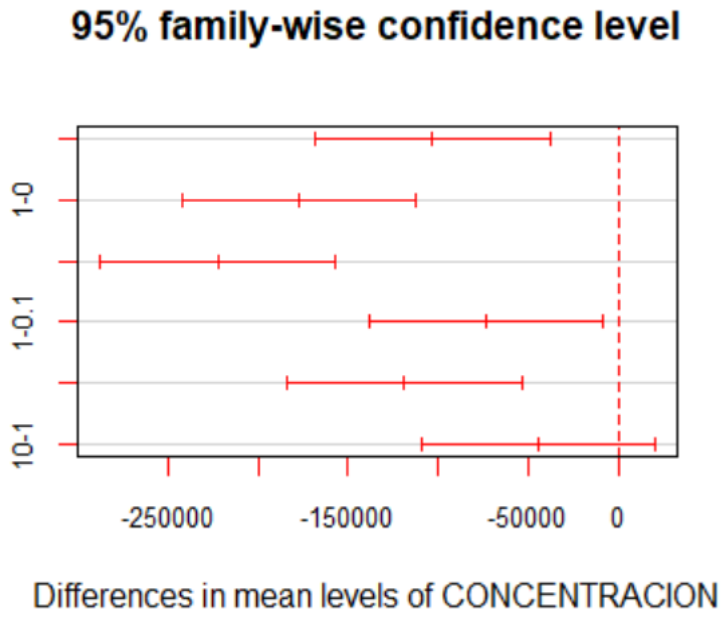

Annex 6. Tukey's test for the treatment of SHSY5Y cells with NDZ.

.

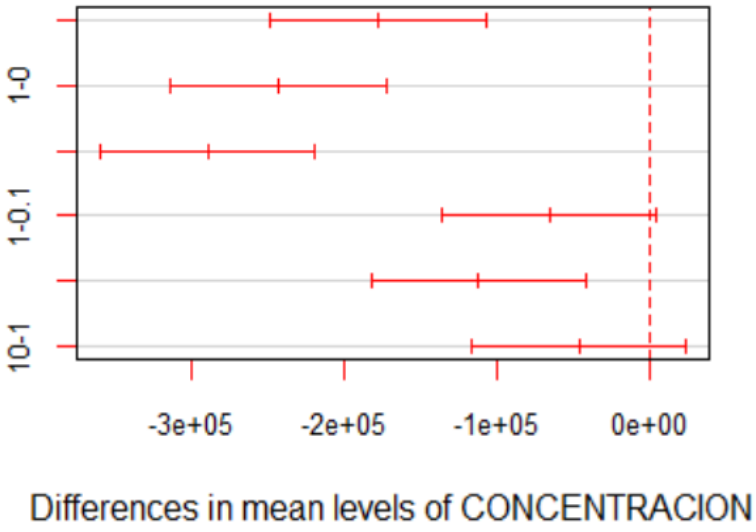

Annex 7. Tukey's test for the treatment of HEK 293 cells with colchicine.

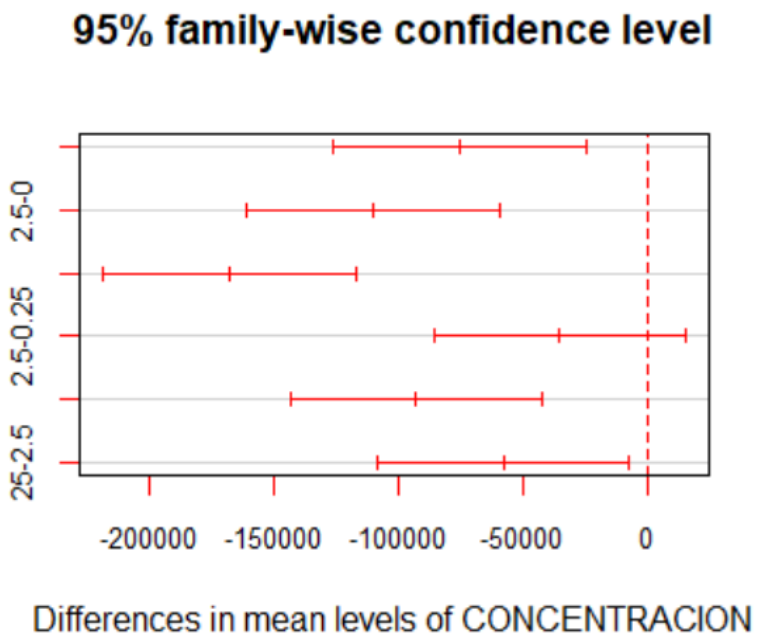

Annex 8. Tukey's test for the treatment of SHSY5Y cells with colchicine.

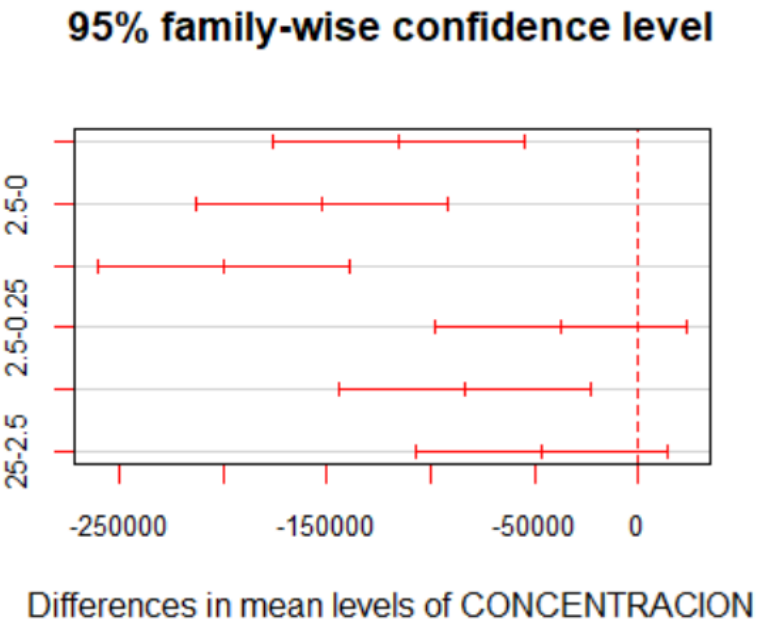

Annex 8. protocol for cell passage

The procedure for 25 cm^2 flask was the following:

1. Remove culture medium.
2. Add PBS to rinse and discard.
3. Add 1.5 ml of trypsin solution, place at 37 °C for 2 minutes.
4. Add 3.5 ml of complete growth medium and aspirate cells by gently pipetting.
5. Centrifuge at 95xg for 3 minutes. Discard the supernatant.
6. Add 4.5 ml to the new flask.
7. Suspend the centrifuged cells in 3 ml of complete medium growth, take 0.5 ml, and add to a new flask.
8. Incubate cultures at 37°C with an atmosphere composed of 95% air, 5% (CO_2).

Annex 9. Protocol and code for computing of fluorescence density.

Code in Python

```
# Read image as gray scale.
gray_img = cv2.imread("/content/drive/MyDrive/máscara/imágenes/control
_63x.jpg", 0) # images/imagen_pacli_63x.jpg

mask = cv2.adaptiveThreshold(gray_img, 255, cv2.ADAPTIVE_THRESH_MEAN_C
, cv2.THRESH_BINARY, 199, -8) / 255.0
mask_gray = np.multiply(gray_img, mask)
density = np.sum(mask_gray) / np.sum(mask)
print("Density: ", density)

fig, axs = plt.subplots(figsize = (40, 30))
```

```
plt.subplot(1, 3, 1)
plt.imshow(gray_img, cmap = 'Greens')
plt.title('Original')

plt.subplot(1, 3, 2)
plt.imshow(mask, cmap = 'gray') #
plt.title('Mask')

plt.subplot(1, 3, 3)
plt.imshow(mask_gray, cmap = 'Greens')
plt.title('Masked gray image')
```

```
Density:  103.30942110095205
```

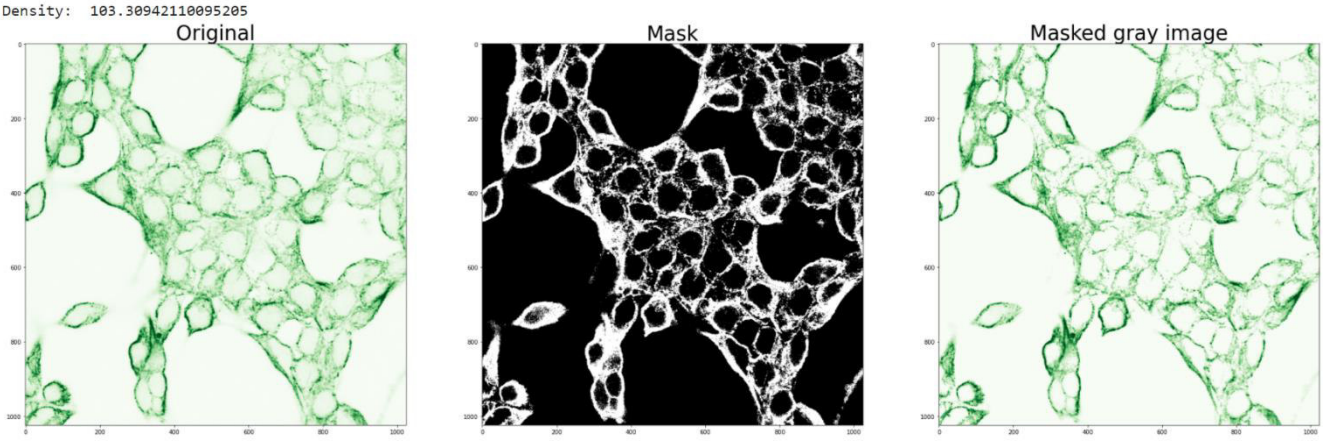

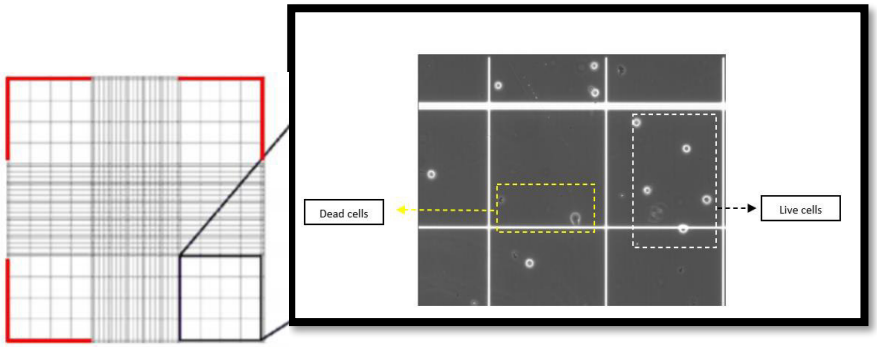

photo of dead and living cells observed in the hemocytometer

For the cell count the following formula was used:

$$concentrationcell/ml) = \frac{n°alivecell}{n°countedquadrants} * dilutionfactor$$

In this case, *dilution factor was 2.*

Annex 11.1 Data of survival HEK 293 cells (NUM.CELL in the table) treated with PTX.

CONCENTRATION (nM)	TIME (hr)	NUM.CELL
1.25	12	220000
1.25	12	210000
1.25	12	235000
1.25	24	150000
1.25	24	165000
1.25	24	185000
1.25	36	135000
1.25	36	140000
1.25	36	150000
2.5	12	135000
2.5	12	150000
2.5	12	165000
2.5	24	120000
2.5	24	135000
2.5	24	150000
2.5	36	105000
2.5	36	115000
2.5	36	120000
5	12	110000
5	12	125000
5	12	135000
5	24	110000
5	24	115000
5	24	120000
5	36	55000
5	36	75000
5	36	90000
0	12	245000
0	12	255000
0	12	265000
0	24	380000
0	24	400000
0	24	410000
0	36	580000
0	36	605000
0	36	615000

Annex 11.2 Data of survival HEK 293 cells (NUM.CELL in the table) treated with Epo B.

CONCENTRATION (nM)	TIME (hr)	NUM.CELL
0.3	15	280000
0.3	15	260000
0.3	15	275000
0.3	20	255000
0.3	20	240000
0.3	20	265000
0.3	25	205000
0.3	25	215000
0.3	25	195000
3	15	145000
3	15	130000
3	15	155000
3	20	110000
3	20	135000
3	20	100000
3	25	85000
3	25	105000
3	25	90000
30	15	95000
30	15	105000
30	15	110000
30	20	75000
30	20	90000
30	20	85000
30	25	55000
30	25	65000
30	25	40000
0	15	290000
0	15	295000
0	15	285000
0	20	380000
0	20	362500
0	20	350000
0	25	395000
0	25	410000
0	25	420000

Annex 11.3 Data of survival HEK 293 cells (NUM.CELL in the table) treated with Colchicine.

CONCENTRATION (μM)	TIME (hr)	NUM.CELL
0.25	4	235000
0.25	4	215000
0.25	4	205000
0.25	8	195000
0.25	8	210000
0.25	8	180000
0.25	12	140000
0.25	12	160000
0.25	12	130000
2.5	4	210000
2.5	4	230000
2.5	4	195000
2.5	8	135000
2.5	8	155000
2.5	8	125000
2.5	12	100000
2.5	12	110000
2.5	12	95000
25	4	140000
25	4	155000
25	4	135000
25	8	75000
25	8	90000
25	8	85000
25	12	50000
25	12	65000
25	12	40000
0	4	215000
0	4	240000
0	4	225000
0	8	262500
0	8	280000
0	8	255000
0	12	295000
0	12	290000
0	12	285000

Annex 11.4 Data of survival HEK 293 cells (NUM.CELL in the table) treated with NDZ.

CONCENTRATION (μM)	TIME (hr)	NUM.CELL
0.1	5	250000
0.1	5	260000
0.1	5	230000
0.1	11	210000
0.1	11	215000
0.1	11	190000
0.1	18	165000
0.1	18	175000
0.1	18	145000
1	5	200000
1	5	215000
1	5	185000
1	11	125000
1	11	140000
1	11	110000
1	18	65000
1	18	80000
1	18	55000
10	5	165000
10	5	175000
10	5	145000
10	11	70000
10	11	80000
10	11	55000
10	18	25000
10	18	35000
10	18	20000
0	5	275000
0	5	280000
0	5	260000
0	11	295000
0	11	285000
0	11	300000
0	18	355000
0	18	370000
0	18	350000

Annex 11.5 Data of survival SHSY5Y cells (NUM.CELL in the table) treated with PTX.

CONCENTRATION (nM)	TIME (hr)	NUM.CELL
1.25	12	160000
1.25	12	230000
1.25	12	210000
1.25	24	120000
1.25	24	195000
1.25	24	150000
1.25	36	55000
1.25	36	140000
1.25	36	100000
2.5	12	130000
2.5	12	160000
2.5	12	150000
2.5	24	70000
2.5	24	145000
2.5	24	105000
2.5	36	45000
2.5	36	110000
2.5	36	85000
5	12	100000
5	12	125000
5	12	115000
5	24	50000
5	24	115000
5	24	90000
5	36	35000
5	36	90000
5	36	65000
0	12	225000
0	12	205000
0	12	215000
0	24	265000
0	24	325000
0	24	310000
0	36	415000
0	36	330000
0	36	380000

Annex 11.6 Data of survival SHSY5Y cells (NUM.CELL in the table) treated with Epo B.

CONCENTRATION (nM)	TIME (hr)	NUM.CELL
0.3	15	170000
0.3	15	185000
0.3	15	195000
0.3	20	140000
0.3	20	130000
0.3	20	150000
0.3	25	105000
0.3	25	95000
0.3	25	110000
3	15	125000
3	15	135000
3	15	140000
3	20	115000
3	20	100000
3	20	120000
3	25	90000
3	25	80000
3	25	75000
30	15	95000
30	15	125000
30	15	115000
30	20	85000
30	20	75000
30	20	90000
30	25	45000
30	25	30000
30	25	40000
0	15	335000
0	15	345000
0	15	320000
0	20	390000
0	20	375000
0	20	380000
0	25	445000
0	25	420000
0	25	425000

Annex 11.7 Data of survival SHSY5Y cells (NUM.CELL in the table) treated with Colchicine.

CONCENTRATION (μM)	TIME (hr)	NUM.CELL
0.25	4	375000
0.25	4	390000
0.25	4	380000
0.25	8	315000
0.25	8	325000
0.25	8	310000
0.25	12	280000
0.25	12	260000
0.25	12	300000
2.5	4	335000
2.5	4	350000
2.5	4	320000
2.5	8	290000
2.5	8	275000
2.5	8	260000
2.5	12	245000
2.5	12	270000
2.5	12	255000
25	4	280000
25	4	285000
25	4	290000
25	8	235000
25	8	245000
25	8	250000
25	12	175000
25	12	215000
25	12	205000
0	4	395000
0	4	370000
0	4	405000
0	8	440000
0	8	410000
0	8	395000
0	12	550000
0	12	515000
0	12	495000

Annex 11.8 Data of survival SHSY5Y cells (NUM.CELL in the table) treated with NDZ.

CONCENTRATION (μM)	TIME (hr)	NUM.CELL
0.1	5	315000
0.1	5	325000
0.1	5	335000
0.1	11	290000
0.1	11	270000
0.1	11	305000
0.1	18	200000
0.1	18	230000
0.1	18	185000
1	5	250000
1	5	225000
1	5	260000
1	11	205000
1	11	235000
1	11	195000
1	18	160000
1	18	185000
1	18	150000
10	5	205000
10	5	190000
10	5	215000
10	11	170000
10	11	190000
10	11	155000
10	18	130000
10	18	100000
10	18	95000
0	5	365000
0	5	380000
0	5	395000
0	11	440000
0	11	425000
0	11	415000
0	18	550000
0	18	565000
0	18	520000

References

[1] R. Romaniello *et al.*, "Tubulin genes and malformations of cortical development," *Eur. J. Med. Genet.*, vol. 61, no. 12, pp. 744–754, Dec. 2018, doi: 10.1016/J.EJMG.2018.07.012.

[2] S. Chakraborti, K. Natarajan, J. Curiel, C. Janke, and J. Liu, "The emerging role of the tubulin code: From the tubulin molecule to neuronal function and disease," *Cytoskeleton*, vol. 73, no. 10, pp. 521–550, Oct. 2016, doi: 10.1002/CM.21290.

[3] M. S. Van Der Knaap *et al.*, "Hypomyelination with atrophy of the basal ganglia and cerebellum: Follow-up and pathology," *Neurology*, vol. 69, no. 2, pp. 166–171, Jul. 2007, doi: 10.1212/01.wnl.0000265592.74483.a6.

[4] M. S. van der Knaap *et al.*, "New Syndrome Characterized by Hypomyelination with Atrophy of the Basal Ganglia and Cerebellum," *AJNR Am. J. Neuroradiol.*, vol. 23, no. 9, p. 1466, Oct. 2002, Accessed: Aug. 23, 2021. [Online]. Available: /pmc/articles/PMC7976795/.

[5] A. Lopez-Juarez *et al.*, "Auditory impairment in H-ABC tubulinopathy," *J. Comp. Neurol.*, vol. 529, no. 5, pp. 957–968, Apr. 2021, doi: 10.1002/CNE.24990.

[6] I. D. Duncan, K. F. Lunn, B. Holmgren, R. Urba-Holmgren, and L. Brignolo-Holmes, "The taiep rat: A myelin mutant with an associated oligodendrocyte microtubular defect," *J. Neurocytol.*, vol. 21, no. 12, pp. 870–884, Dec. 1992, doi: 10.1007/BF01191684.

[7] I. D. Duncan *et al.*, "A mutation in the Tubb4a gene leads to microtubule accumulation with hypomyelination and demyelination," *Ann. Neurol.*, vol. 81, no. 5, pp. 690–702, 2017, doi: 10.1002/ana.24930.

[8] Y. Lu, Y. Ondo, K. Shimojima, H. Osaka, and T. Yamamoto, "A novel TUBB4A mutation G96R identified in a patient with hypomyelinating leukodystrophy onset beyond adolescence," *Hum. Genome Var.*, vol. 4, Aug. 2017, doi: 10.1038/hgv.2017.35.

[9] D. Bates and A. Eastman, "Microtubule destabilising agents: far more than just antimitotic anticancer drugs," *Br. J. Clin. Pharmacol.*, vol. 83, no. 2, p. 255, 2017, doi: 10.1111/BCP.13126.

[10] R. Zhang, G. M. Alushin, A. Brown, and E. Nogales, "Mechanistic origin of microtubule dynamic instability and its modulation by EB proteins," *Cell*, vol. 162, no. 4, pp. 849–859, Aug. 2015, doi: 10.1016/j.cell.2015.07.012.

[11] J. Boyle, "Molecular biology of the cell, 5th edition by B. Alberts, A. Johnson, J. Lewis, M. Raff, K. Roberts, and P. Walter," *Biochem. Mol. Biol. Educ.*, vol. 36, no. 4, pp. 317–318, Jul. 2008, doi: 10.1002/BMB.20192.

[12] *The Role of Microtubules in Cell Biology, Neurobiology, and Oncology*. Humana Press, 2008.

[13] T. Mitchison and M. Kirschner, "Dynamic instability of microtubule growth," *Nature*, vol. 312, no. 5991, pp. 237–242, 1984, doi: 10.1038/312237a0.

[14] M. F. Carlier, T. L. Hill, and Y. D. Chen, "Interference of GTP hydrolysis in the mechanism of microtubule assembly: An experimental study," *Proc. Natl. Acad. Sci. U. S. A.*, vol. 81, no. 3 I, pp. 771–775, 1984, doi: 10.1073/pnas.81.3.771.

[15] G. Bhabha, G. T. Johnson, C. M. Schroeder, and R. D. Vale, ‘‘How dynein moves along microtubules,’’ *Trends Biochem. Sci.*, vol. 41, no. 1, p. 94, Jan. 2016, doi: 10.1016/J.TIBS.2015.11.004.

[16] F. J. McNally and A. Roll-Mecak, ‘‘Microtubule-severing enzymes: From cellular functions to molecular mechanism,’’ *J. Cell Biol.*, vol. 217, no. 12, pp. 4057–4069, Dec. 2018, doi: 10.1083/JCB.201612104.

[17] R. J and S. T, ‘‘Microtubule nucleation: beyond the template,’’ *Nat. Rev. Mol. Cell Biol.*, vol. 18, no. 11, pp. 702–710, 2017, doi: 10.1038/NRM.2017.75.

[18] A. Akhmanova and C. C. Hoogenraad, ‘‘Microtubule Minus-End-Targeting Proteins,’’ *Curr. Biol.*, vol. 25, no. 4, pp. R162–R171, Feb. 2015, doi: 10.1016/J.CUB.2014.12.027.

[19] H. T, ‘‘Microtubule organization and microtubule-associated proteins in plant cells,’’ *Int. Rev. Cell Mol. Biol.*, vol. 312, pp. 1–52, 2014, doi: 10.1016/B978-0-12-800178-3.00001-4.

[20] S. Bodakuntla, A. S. Jijumon, C. Villablanca, C. Gonzalez-Billault, and C. Janke, ‘‘Microtubule-Associated Proteins: Structuring the Cytoskeleton,’’ *Trends Cell Biol.*, vol. 29, no. 10, pp. 804–819, Oct. 2019, doi: 10.1016/J.TCB.2019.07.004.

[21] C. Sander and R. Schneider, ‘‘Database of homology-derived protein structures and the structural meaning of sequence alignment,’’ *Proteins Struct. Funct. Bioinforma.*, vol. 9, no. 1, pp. 56–68, 1991, doi: 10.1002/prot.340090107.

[22] E. Nogales and H. W. Wang, ‘‘Structural intermediates in microtubule assembly and disassembly: How and why?,’’ *Current Opinion in Cell Biology*, vol. 18, no. 2. Curr Opin Cell Biol, pp. 179–184, Apr. 2006, doi: 10.1016/j.ceb.2006.02.009.

[23] ‘‘Three dimensional structure of tubulin heterodimer (abTub), gamma... | Download Scientific Diagram.’’ https://www.researchgate.net/figure/Three-dimensional-structure-of-tubulin-heterodimer-abTub-gamma-synuclein-gSyn-and_fig1_236083854 (accessed Nov. 13, 2021).

[24] M. A. Tischfield, G. Y. Cederquist, M. L. Gupta, and E. C. Engle, ‘‘Phenotypic spectrum of the tubulin-related disorders and functional implications of disease-causing mutations,’’ *Current Opinion in Genetics and Development*, vol. 21, no. 3. NIH Public Access, pp. 286–294, Jun. 2011, doi: 10.1016/j.gde.2011.01.003.

[25] S. Uchimura *et al.*, ‘‘Identification of a strong binding site for kinesin on the microtubule using mutant analysis of tubulin,’’ *EMBO J.*, vol. 25, no. 24, pp. 5932–5941, Dec. 2006, doi: 10.1038/sj.emboj.7601442.

[26] S. Uchimura, Y. Oguchi, Y. Hachikubo, S. Ishiwata, and E. Muto, ‘‘Key residues on microtubule responsible for activation of kinesin ATPase,’’ *EMBO J.*, vol. 29, no. 7, pp. 1167–1175, Apr. 2010, doi: 10.1038/emboj.2010.25.

[27] J. Löwe, H. Li, K. H. Downing, and E. Nogales, ‘‘Refined structure of αβ-tubulin at 3.5 Å resolution,’’ *J. Mol. Biol.*, vol. 313, no. 5, pp. 1045–1057, Nov. 2001, doi: 10.1006/jmbi.2001.5077.

[28] C. E. Walczak, S. Cai, and A. Khodjakov, ‘‘Mechanisms of chromosome behaviour during mitosis,’’ *Nat. Rev. Mol. Cell Biol.*, vol. 11, no. 2, p. 91, Feb. 2010, doi: 10.1038/NRM2832.

[29] N. M. Rusan, C. J. Fagerstrom, A.-M. C. Yvon, and P. Wadsworth, ‘‘Cell Cycle-Dependent Changes in Microtubule Dynamics in Living Cells Expressing Green Fluorescent Protein-α Tubulin182,” *https://doi.org/10.1091/mbc.12.4.971*, vol. 12, no. 4, pp. 971–980, Oct. 2017, doi: 10.1091/MBC.12.4.971.

[30] H. JH, B. SS, and R. CL, ‘‘Kinetochores capture astral microtubules during chromosome attachment to the mitotic spindle: direct visualization in live newt lung cells,” *J. Cell Biol.*, vol. 111, no. 3, pp. 1039–1045, 1990, doi: 10.1083/JCB.111.3.1039.

[31] M. A. Jordan and L. Wilson, ‘‘Microtubules as a target for anticancer drugs,” *Nat. Rev. Cancer*, vol. 4, no. 4, pp. 253–265, 2004, doi: 10.1038/NRC1317.

[32] M. A. Jordan, R. J. Toso, D. Thrower, and L. Wilson, ‘‘Mechanism of mitotic block and inhibition of cell proliferation by taxol at low concentrations,” *Proc. Natl. Acad. Sci.*, vol. 90, no. 20, pp. 9552–9556, Oct. 1993, doi: 10.1073/PNAS.90.20.9552.

[33] J. Zhou and P. Giannakakou, ‘‘Targeting microtubules for cancer chemotherapy,” *Curr. Med. Chem. - Anti-Cancer Agents*, vol. 5, no. 1, pp. 65–71, Jan. 2005, doi: 10.2174/1568011053352569.

[34] N. RL, B. CT, and C. JH, ‘‘Role of chance observations in chemotherapy: Vinca rosea,” *Ann. N. Y. Acad. Sci.*, vol. 76, no. 3, pp. 882–894, 1958, doi: 10.1111/J.1749-6632.1958.TB54906.X.

[35] D. C and J. MA, ‘‘Microtubule-binding agents: a dynamic field of cancer therapeutics,” *Nat. Rev. Drug Discov.*, vol. 9, no. 10, pp. 790–803, 2010, doi: 10.1038/NRD3253.

[36] D. JF and A. JM, ‘‘Assembly of purified GDP-tubulin into microtubules induced by taxol and taxotere: reversibility, ligand stoichiometry, and competition,” *Biochemistry*, vol. 32, no. 11, pp. 2747–2755, Mar. 1993, doi: 10.1021/BI00062A003.

[37] F. S and M. TJ, ‘‘Anti-Microtubule Drugs,” *Methods Mol. Biol.*, vol. 1413, pp. 403–421, 2016, doi: 10.1007/978-1-4939-3542-0_25.

[38] R. A. Stanton, K. M. Gernert, J. H. Nettles, and R. Aneja, ‘‘Drugs that target dynamic microtubules: A new molecular perspective,” *Med. Res. Rev.*, vol. 31, no. 3, pp. 443–481, May 2011, doi: 10.1002/med.20242.

[39] G. M. Alushin, G. C. Lander, E. H. Kellogg, R. Zhang, D. Baker, and E. Nogales, ‘‘High-Resolution microtubule structures reveal the structural transitions in αβ-tubulin upon GTP hydrolysis,” *Cell*, vol. 157, no. 5, pp. 1117–1129, May 2014, doi: 10.1016/j.cell.2014.03.053.

[40] E. H. Kellogg *et al.*, ‘‘Insights into the Distinct Mechanisms of Action of Taxane and Non-Taxane Microtubule Stabilizers from Cryo-EM Structures,” *J. Mol. Biol.*, vol. 429, no. 5, pp. 633–646, Mar. 2017, doi: 10.1016/j.jmb.2017.01.001.

[41] J. P. Snyder, J. H. Nettles, B. Cornett, K. H. Downing, and E. Nogales, ‘‘The binding conformation of Taxol in β-tubulin: A model based on electron crystallographic density,” *Proc. Natl. Acad. Sci.*, vol. 98, no. 9, pp. 5312–5316, Apr. 2001, doi: 10.1073/PNAS.051309398.

[42] K. Kamath and M. A. Jordan, ‘‘Suppression of microtubule dynamics by epothilone B is associated with mitotic arrest,” *Cancer Res.*, vol. 63, no. 18, pp. 6026–6031, Sep. 2003, Accessed: Dec. 06, 2020. [Online]. Available: https://pubmed.ncbi.nlm.nih.gov/14522931/.

[43] D. M. Bollag *et al.*, ‘‘Epothilones, a New Class of Microtubule-stabilizing Agents with a Taxol-like Mechanism of Action,” *CANCER Res.*, vol. 55, pp. 2325–2333, 1995.

[44] T.-C. Chou *et al.*, ‘‘Desoxyepothilone B is curative against human tumor xenografts that are refractory to paclitaxel,” *Proc. Natl. Acad. Sci. U. S. A.*, vol. 95, no. 26, p. 15798, Dec. 1998, doi: 10.1073/PNAS.95.26.15798.

[45] M. L. Gupta, C. J. Bode, G. I. Georg, and R. H. Himes, ‘‘Understanding tubulin–Taxol interactions: Mutations that impart Taxol binding to yeast tubulin,” *Proc. Natl. Acad. Sci.*, vol. 100, no. 11, pp. 6394–6397, May 2003, doi: 10.1073/PNAS.1131967100.

[46] J. H. Nettles, H. Li, B. Cornett, J. M. Krahn, J. P. Snyder, and K. H. Downing, ‘‘The Binding Mode of Epothilone A on α,ß-Tubulin by Electron Crystallography,” *Science (80-.).*, vol. 305, no. 5685, pp. 866–869, Aug. 2004, doi: 10.1126/SCIENCE.1099190.

[47] R. AR *et al.*, ‘‘Characterizing the Epothilone Binding Site on β-Tubulin by Photoaffinity Labeling: Identification of β-Tubulin Peptides TARGSQQY and TSRGSQQY as Targets of an Epothilone Photoprobe for Polymerized Tubulin,” *J. Med. Chem.*, vol. 59, no. 7, pp. 3499–3514, Apr. 2016, doi: 10.1021/ACS.JMEDCHEM.6B00188.

[48] A. Jordan, J. A. Hadfield, N. J. Lawrence, and A. T. Mcgown, ‘‘Tubulin as a Target for Anticancer Drugs:Agents Which Interact with the Mitotic Spindle,” *Inc. Med. Res. Rev*, vol. 18, no. 4, pp. 259–296, 1997.

[49] A. E. Prota *et al.*, ‘‘The Novel Microtubule-Destabilizing Drug BAL27862 Binds to the Colchicine Site of Tubulin with Distinct Effects on Microtubule Organization,” *J. Mol. Biol.*, vol. 426, no. 8, pp. 1848–1860, Apr. 2014, doi: 10.1016/J.JMB.2014.02.005.

[50] Y. Y. Chao, C. R. Jan, Y. C. Ko, J. J. Chen, and I. S. Chen, ‘‘Interaction of nocodazole with tubulin isotypes,” *Drug Dev. Res.*, vol. 55, no. 2, pp. 91–96, Feb. 2002, doi: 10.1002/ddr.10023.

[51] M. A. Jordan, D. Thrower, and L. Wilson, ‘‘Effects of vinblastine, podophyllotoxin and nocodazole on mitotic spindles Implications for the role of microtubule dynamics in mitosis,” *J. Cell Sci.*, vol. 102, pp. 401–416, 1992.

[52] J. Chen, T. Liu, X. Dong, and Y. Hu, ‘‘Recent Development and SAR Analysis of Colchicine Binding Site Inhibitors,” *Mini-Reviews Med. Chem.*, vol. 9, no. 10, pp. 1174–1190, Aug. 2009, doi: 10.2174/138955709789055234.

[53] A.-O. R *et al.*, ‘‘Towards the identification of the binding site of benzimidazoles to β-tubulin of Trichinella spiralis: insights from computational and experimental data,” *J. Mol. Graph. Model.*, vol. 41, pp. 12–19, Apr. 2013, doi: 10.1016/J.JMGM.2013.01.007.

[54] W. Y *et al.*, ‘‘Structures of a diverse set of colchicine binding site inhibitors in complex with tubulin provide a rationale for drug discovery,” *FEBS J.*, vol. 283, no. 1, pp. 102–111, Jan. 2016, doi: 10.1111/FEBS.13555.

[55] Y. Y. Leung, L. L. Y. Hui, and V. B. Kraus, ‘‘Colchicine --- update on mechanisms of action and therapeutic uses,” *Semin. Arthritis Rheum.*, vol. 45, no. 3, p. 341, Dec. 2015, doi: 10.1016/J.SEMARTHRIT.2015.06.013.

[56] H. R. Xie, L. Sen Hu, and G. Y. Li, ‘‘SH-SY5Y human neuroblastoma cell line: In vitro cell model of dopaminergic neurons in Parkinson’s disease,” *Chin. Med. J. (Engl).*, vol. 123, no. 8, pp.

1086–1092, 2010, doi: 10.3760/CMA.J.ISSN.0366-6999.2010.08.021.

[57] Z. Xun *et al.*, ‘‘Retinoic acid-induced differentiation increases the rate of oxygen consumption and enhances the spare respiratory capacity of mitochondria in SH-SY5Y cells,” *Mech. Ageing Dev.*, vol. 133, no. 4, p. 176, Apr. 2012, doi: 10.1016/J.MAD.2012.01.008.

[58] J. Song, L. T. O’connor, W. Yu, P. W. Baas, and I. D. Duncan, ‘‘Microtubule alterations in cultured taiep rat oligodendrocytes lead to deficits in myelin membrane formation,” *J. Neurocytol. 1999 288*, vol. 28, no. 8, pp. 671–684, 1999, doi: 10.1023/A:1007060832459.

[59] J. Curiel *et al.*, ‘‘TUBB4A mutations result in specific neuronal and oligodendrocytic defects that closely match clinically distinct phenotypes,” *Hum. Mol. Genet.*, vol. 26, no. 22, pp. 4506–4518, Nov. 2017, doi: 10.1093/hmg/ddx338.

[60] A. Garduno-Robles *et al.*, ‘‘MRI Features in a Rat Model of H-ABC Tubulinopathy,” *Front. Neurosci.*, vol. 14, p. 555, Jun. 2020, doi: 10.3389/fnins.2020.00555.

[61] E. R. Jose, C. Ma del Carmen, U. Araceli, and L.-C. Alicia, ‘‘The Myelin Mutant Rat Taiep as a Model of Neuroimmunological Disease,” *Adv. Neuroimmune Biol.*, vol. 5, pp. 9–17, 2014, doi: 10.3233/NIB-140081.

[62] J. Song, B. D. Goetz, P. W. Baas, and L. D. Duncan, ‘‘Cytoskeletal Reorganization during the Formation of Oligodendrocyte Processes and Branches,” *Mol. Cell. Neurosci.*, vol. 17, no. 4, pp. 624–636, Apr. 2001, doi: 10.1006/MCNE.2001.0974.

[63] F. Borys, E. Joachimiak, H. Krawczyk, and H. Fabczak, ‘‘molecules Intrinsic and Extrinsic Factors Affecting Microtubule Dynamics in Normal and Cancer Cells,” doi: 10.3390/molecules25163705.

[64] R. F. Ludueña, ‘‘Are tubulin isotypes functionally significant,” *Mol. Biol. Cell*, vol. 4, no. 5, pp. 445–457, 1993, doi: 10.1091/mbc.4.5.445.

[65] D. Raybin1 and M. Flavin, ‘‘Enzyme Which Specifically Adds Tyrosine to the a Chain of Tubulin?”

[66] L. Peris *et al.*, ‘‘Tubulin tyrosination is a major factor affecting the recruitment of CAP-Gly proteins at microtubule plus ends,” *J. Cell Biol.*, vol. 174, no. 6, p. 839, Sep. 2006, doi: 10.1083/JCB.200512058.

[67] T. J. Hausrat, J. Radwitz, F. L. Lombino, P. Breiden, and M. Kneussel, ‘‘Alpha- and beta-tubulin isotypes are differentially expressed during brain development,” *Dev. Neurobiol.*, vol. 81, no. 3, pp. 333–350, Apr. 2021, doi: 10.1002/DNEU.22745.

[68] J. Guo, C. Walss-Bass, and R. F. Ludueña, ‘‘The β isotypes of tubulin in neuronal differentiation,” *Cytoskeleton (Hoboken).*, vol. 67, no. 7, p. 431, Jul. 2010, doi: 10.1002/CM.20455.

[69] ‘‘Search: SH-SY5Y cells - The Human Protein Atlas.” https://www.proteinatlas.org/search/SH-SY5Y+cells (accessed Oct. 28, 2021).

[70] D. W. Cleveland, M. A. Lopata, P. Sherunes, and M. W. Kirschner, ‘‘Unpolymerized Tubulin Modulates the Level of Tubulin mRNAs,” *Cell*, vol. 25, pp. 537–546, 1981.

[71] E. MASUROVSKY, E. PETERSON, S. CRAIN, and S. HORWITZ, ‘‘Taxol effects on GLIA in

organotypic mouse spinal cord-DRG cultures," *Cell Biol. Int. Rep.*, vol. 9, no. 6, pp. 539–546, Jun. 1985, doi: 10.1016/0309-1651(85)90018-9.

[72] "Four-stranded mini microtubules formed by Prosthecobacter BtubAB show dynamic instability. | Centro de Investigaciones Biológicas Margarita Salas - CIB Margarita Salas." https://www.cib.csic.es/es/events/four-stranded-mini-microtubules-formed-prosthecobacter-btubab-show-dynamic-instability-0 (accessed Oct. 05, 2021).

[73] D. Tong and G. A. Voth, "Microtubule Simulations Provide Insight into the Molecular Mechanism Underlying Dynamic Instability," *Biophys. J.*, vol. 118, no. 12, pp. 2938–2951, Jun. 2020, doi: 10.1016/J.BPJ.2020.04.028.

[74] G. M. Alushin, G. C. Lander, E. H. Kellogg, R. Zhang, D. Baker, and E. Nogales, "High resolution microtubule structures reveal the structural transitions in αβ–tubulin upon GTP hydrolysis," *Cell*, vol. 157, no. 5, p. 1117, May 2014, doi: 10.1016/J.CELL.2014.03.053.

[75] L. G. Hevia and M. L. Fanarraga, "Microtubule cytoskeleton-disrupting activity of MWCNTs: applications in cancer treatment," *J. Nanobiotechnology*, vol. 18, no. 1, Dec. 2020, doi: 10.1186/S12951-020-00742-Y.

[76] D. Bates and A. Eastman, "Microtubule destabilising agents: far more than just antimitotic anticancer drugs," *British Journal of Clinical Pharmacology*, vol. 83, no. 2. Blackwell Publishing Ltd, pp. 255–268, 2017, doi: 10.1111/bcp.13126.

[77] K. Y. Park, S. Kim, and M. S. Kim, "Effects of taxol on neuronal differentiation of postnatal neural stem cells cultured from mouse subventricular zone," *Differentiation*, vol. 119, no. April, pp. 1–9, 2021, doi: 10.1016/j.diff.2021.03.001.

[78] Reyes-Haro, D., Mora-Loyola, E., Soria-Ortiz, B., & García-Colunga, J. (2013). Regional density of glial cells in the rat corpus callosum. *Biological Research*, *46*(1) 27–32. https://doi.org/10.4067/S0716-97602013000100004.

Cartas de los sinodales

UNIVERSIDAD DE GUANAJUATO
DIVISIÓN DE CIENCIAS NATURALES Y EXACTAS
DEPARTAMENTO DE FARMACIA

Col. Noria Alta S/N 36050 Guanajuato, Gto., México Tel.: 01 (473) 732-00-06, Ext. 8125, Fax: Ext.: 8108

Guanajuato, Gto. 26 de noviembre de 2021

Asunto: Carta de aceptación de tesis

Dr. Davis Yves Ghislain Delepine
Director de la División de Ciencias e Ingenierías
Campus León
Universidad de Guanajuato

Dr. David Delepine:

Por medio de la presente, informo a usted que he leído el manuscrito de tesis de la estudiante de la Maestría en Ciencias Aplicadas de la DCI, Ing. Biomédica Carla María Jaramillo Restrepo, la cual lleva por título: "BIOPHOTONIC AND MOLECULAR ANALYSIS OF TUBULINOPATHIES".

Después de haber realizado mis comentarios, la estudiante realizó las correcciones pertinentes, además de que es un trabajo desarrollado con la calidad y el rigor científico requerido para una tesis de maestría. Por lo anterior doy mi consentimiento para que Carla María Jaramillo Restrepo, defienda de manera oral su tesis de Maestría en la fecha que sus directores de tesis juzguen conveniente.

Sin más por el momento, y agradeciendo las atenciones a la presente, me despido enviando un cordial saludo y quedando a sus apreciables órdenes.

Atentamente

Clara Alba Betancourt

Dra. Clara Alba Betancourt
Profesor Asociado C, Tiempo Completo. SNI nivel I
Departamento de Farmacia. Universidad de Guanajuato.
c.albabetancourt@ugto.mx. Tel. 4737320006, ext. 1479.

UNIVERSIDAD DE GUANAJUATO

Dr. Davis Yves Ghislain Delepine
Director de la División de Ciencias e Ingenierías
Campus León
Universidad de Guanajuato

León, Gto., 23 de noviembre del 2021.

Dr. David Delepine:

Por medio de la presente, informo a usted que he leído el manuscrito de tesis de la estudiante de la Maestría en Ciencias Aplicadas de la DCI, Ing. Biomédica **Carla María Jaramillo Restrepo**, la cual lleva por título: **"BIOPHOTONIC AND MOLECULAR ANALYSIS OF TUBULINOPATHIES".**

Después de haber realizado mis comentarios, el estudiante realizó las correcciones pertinentes. Por lo anterior doy mi consentimiento para que Carla María Jaramillo Restrepo, defienda de manera oral su tesis de Maestría en la fecha que sus directores de tesis juzguen conveniente.

Sin más por el momento, y agradeciendo las atenciones a la presente, me despido enviando un cordial saludo.

Atentamente

Dra. Silvia Alejandra López Juárez
Profesor-Investigador

División de Ciencias e Ingenierías
Departamento de Ingeniería Química, Electrónica y Biomédica
Loma del Bosque 103, Col. Lomas del Campestre, León, Gto., CP 37000 Tel. (477) 788 5100 ext. 8493
www.dci.ugto.mx

UNIVERSIDAD AUTÓNOMA METROPOLITANA
Unidad Cuajimalpa

Asunto: Aprobación de trabajo de tesis de Maestría

Ciudad de México, 26 de noviembre del 2021

Dr. David Yves Ghislain Delepine
Directo de la División de Ciencias e Ingenierías
Campus León, Universidad de Guanajuato
PRESENTE

Estimado Dr. David Delepine:

En mi carácter de revisora del trabajo de tesis de Maestría presentado por la Ingeniera Biomédica **Carla Jaramillo Restrepo,** para optar por el grado de Maestra en Ciencias Aplicadas de la DCI y cuyo título es: **"Biophotonic and Molecular Analysis of Tubulinopathies"**; me permito comunicarle que después de haber hecho mis comentarios, la estudiante realizó las correcciones pertinentes. Por lo que considero que dicha tesis reúne los requisitos y méritos suficientes para poder continuar con sus trámites de solicitud de examen de grado, en la fecha que sus directores de tesis consideren pertinente.

Sin más por el momento, agradezco de antemano su atención y aprovecho para enviarle un cordial saludo.

ATENTAMENTE

DRA. CYNTHIA GABRIELA SÁMANO SALAZAR
Profesora Asociada de T.C.
Depto. de Ciencias Naturales (DCN)
Universidad Autónoma Metropolitana, unidad Cuajimalpa

UAM | UNIDAD CUAJIMALPA
Avenida Vasco de Quiroga 4871, Col. Santa Fe Cuajimalpa.
Alcaldía Cuajimalpa C.P. 05348 CDMX. Tel: (55) 5814 6500

Asunto: aprobación de trabajo de tesis

León, Gto., a 26 de noviembre de 2021

DR. DAVID DELEPINE
DIRECTOR DE LA
DIVISIÓN DE CIENCIAS E INGENIERÍAS
UNIVERSIDAD DE GUANAJUATO

En mi carácter de revisor del trabajo de tesis de licenciatura presentado por la alumna **Carla María Jaramillo Restrepo**, para optar por el grado de maestra en Ciencias Aplicadas con el trabajo titulado:

"Biophotonic and molecular analysis of tubulinopathies"

me permito comunicarle que despues de haber revisado y discutido el manuscrito, considero que dicha tesis reúne los requisitos y méritos suficientes para poder continuar con sus trámites de solicitud de examen de grado.

Agradezco mucho su atención y aprovecho para enviarle un saludo cordial.

ATENTAMENTE

Dra. Valeria Piazza

Loma del Bosque No. 115, Col. Lomas del Campestre, C.P. 37150, León, Gto., México.
Tel: (477) 441 4200 Fax: (477) 441 4209 www.cio.mx

UNIVERSIDAD DE GUANAJUATO
Campus León
División de Ciencias e Ingenierías

Oficio número: AGV-2021-11-002
Asunto: Carta conformidad
Tesis de Maestría en Ciencias Aplicadas de Carla María Jaramillo Restrepo.
León Gto., 29 de noviembre de 2021.

Dr. David Yves Ghislain Delepine
Director.
División de Ciencias e Ingenierías Campus León

Estimado Dr. Delepine:

Sirva la presente para hacer de su conocimiento que he revisado el trabajo titulado "**Análisis biofotónico y molecular de tubulinopatías**", cuyo documento de tesis está escrito en idioma inglés bajo el título **"Biophotonic and Molecular Analysis of Tubulinopathies"** que para obtener el grado de Maestra en Ciencias Aplicadas pone a consideración la **Ing. Carla María Jaramillo Restrepo.**

Le comunico que en mi opinión el trabajo reúne las características de nivel y calidad necesarias para una tesis de maestría. Asimismo, he discutido con la Ing. Jaramillo algunos aspectos de su trabajo y le he indicado las correcciones que considero pertinentes, las cuales ha incluido en la versión final del trabajo. De esta manera no tengo objeciones para el desarrollo de su defensa de acuerdo con la reglamentación respectiva.

Agradeciendo la atención prestada a la presente, me despido

A T E N T A M E N T E.
"LA VERDAD OS HARÁ LIBRES"

Dr. Arturo González Vega
Profesor Titular "A"

C.c.p Carla Maria Jaramillo Restrepo.
C.c.p. Archivo AGV.

DEPARTAMENTO DE INGENIERÍAS QUÍMICA, ELECTRÓNICA Y BIOMÉDICA
Lomas del Bosque #103,
Lomas de Campestre, León Gto.
C.P. 37150
(477) 788 5100 Ext. 8435, Fax. Ext. 8410
www.diqeb.ugto.mx